iScience

Article

Fatty acids alter to the toxicity of islet amyloid polypeptide aggregates in a length and saturation dependent manner

Graphical abstract

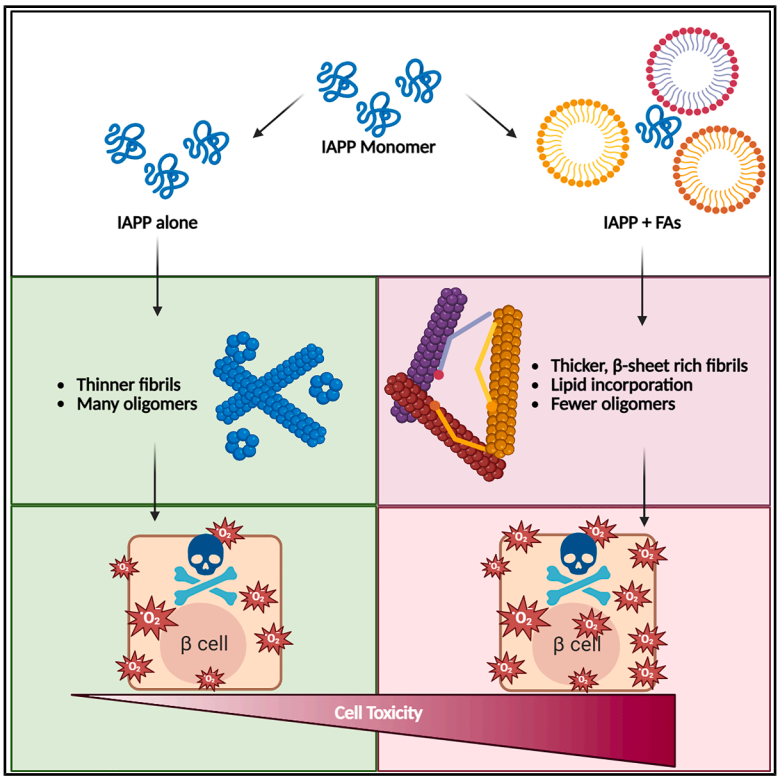

Authors

Jadon Sitton, Davis Pickett, Andrew Hung, Roa Elsaigh, Dmitry Kurouski

Correspondence

dkurouski@tamu.edu

In brief

Molecular biology; Cell biology

Highlights

- Fatty acids accelerate the rate of islet amyloid polypeptide (IAPP) aggregation
- Fatty acids alter the morphology, secondary structure, and toxicity of IAPP fibrils
- Supplementation of FAs to *C. elegans* drastically lowered the lifespan of nematodes

Sitton et al., 2026, iScience *29*, 114401
January 16, 2026
https://doi.org/10.1016/j.isci.2025.114401

CellPress

iScience

CellPress
OPEN ACCESS

Article

Fatty acids alter to the toxicity of islet amyloid polypeptide aggregates in a length and saturation dependent manner

Jadon Sitton,[1] Davis Pickett,[1] Andrew Hung,[1] Roa Elsaigh,[1] and Dmitry Kurouski[1,2,*]
[1]Department of Biochemistry and Biophysics, Texas A&M University, College Station, TX 77843, USA
[2]Lead contact
*Correspondence: dkurouski@tamu.edu
https://doi.org/10.1016/j.isci.2025.114401

SUMMARY

Abrupt the aggregation of islet amyloid polypeptide (IAPP), a 37 amino acid hormone, is an expected molecular cause of type 2 diabetes (T2D), a severe pathology that affects more than 30 million Americans. During the past decade, a significant increase in T2D was observed in children, teens, and young adults. Although this increase is associated with changes in nutrition and lifestyle, its origin remains unclear. Our results indicate that fatty acids often used as food supplements drastically accelerate IAPP aggregation and increase the cytotoxicity of IAPP aggregates. Using *C. elegans* that overexpress IAPP as a model system, we show that an increase in the amount of fatty acids in nematode diets drastically shortens their lifespan. These results indicate that fatty acids present in the diet can accelerate the onset and progression of T2D.

INTRODUCTION

Type 2 diabetes (T2D) is characterized by irreversible insulin resistance, which leads to a state of chronic hyperglycemia.[1] This complex and chronic pathology affects over 520 million people globally as of 2023, and there is currently no definitive cure.[2] One major hallmark of the disease is the accumulation and aggregation of islet amyloid polypeptide (IAPP), a 37 amino acid long peptide hormone that works cooperatively with insulin and glucagon to maintain blood glucose homeostasis.[3,4] Under conditions fostered in T2D, the peptide forms cytotoxic amyloid aggregates and plaques within the insulin-producing β-cells of the pancreas, amplifying the detrimental effects of T2D.[5] Moreover, IAPP aggregation has been observed in the brain, simultaneously facilitating the aggregation of other proteins such as amyloid-β (Aβ) and α-synuclein (α-syn).[6–8] These observations indicate that the onset and progression of Alzheimer's and Parkinson's diseases in patients with T2D could be linked to IAPP aggregation.

In the body, IAPP interacts with numerous biomolecules, including carbohydrates and lipids.[8–10] Zhang et al. found that anionic lipids facilitated the irreversible aggregation of IAPP.[11] Similar findings were reported by Nanga et al. that observed the accelerated formation of a helical intermediate of IAPP in the presence of SDS micelles.[12] These findings suggest that lipid membranes can recruit IAPP to their surfaces and facilitate the formation of intermediates, ultimately accelerating protein aggregation. Ma and coworkers demonstrated that free fatty acids (FAs) facilitated IAPP aggregation in transgenic mice.[13] On the other hand, it has been reported that polyunsaturated FAs (PUFAs) can hinder amyloid formation at higher concentrations.[14] Several groups reported that omega-3 (*n*-3) FAs improved insulin resistance, reduced ER stress, and assisted in mitochondrial maintenance in mice.[15] Furthermore, *n*-3 FAs could lower the risk of Parkinson's and Alzheimer's diseases,[16,17] as well as improve cognitive function.[18] Omega-6 (*n*-6) FAs can lower or alleviate the risk of diabetes depending on what they are bound to,[19,20] emphasizing the importance of understanding the diverse profiles of PUFAs in T2D pathology. Together, evidence has suggested lipids and *n*-3/*n*-6 FAs may have an extensive role in the pathology of T2D and neurodegeneration.

Both *n*-3 and *n*-6 FAs have become more prevalent in food and food supplements. Modern oil sources used in cooking and food production, such as soybean and corn oil, contain high amounts of linoleic acid (LA), an *n*-6 essential fatty acid. Consumption of these oils has increased the amount of LA consumed by humans over 3-fold, increasing the overall contribution of linoleic acid in consumed calories from 1 to 2% to over 7% in recent years.[21] Excess consumption of LA has been linked to an increased risk of obesity, cardiovascular disease, dementia, type 2 diabetes, and cancer, according to recent studies.[22] Moreover, the ratio of *n*-6/*n*-3 FAs is important to metabolic homeostasis. Specifically, the excessive consumption of *n*-6 FAs can disrupt mitochondrial homeostasis, disrupt the proper localization of *n*-3 FAs, and increase the amount of low-density lipoprotein cholesterol produced by an individual.[23] Previous studies reported by our group showed that PUFAs lowered the stability of amyloidogenic proteins and altered the toxicity of amyloid oligomers and fibrils. Specifically, Hoover and co-workers found that long chain PUFAs accelerated insulin aggregation, as well as increased the toxicity of insulin fibrils.[24] Similar findings were made by Ali and co-workers for α-syn fibrils formed in the

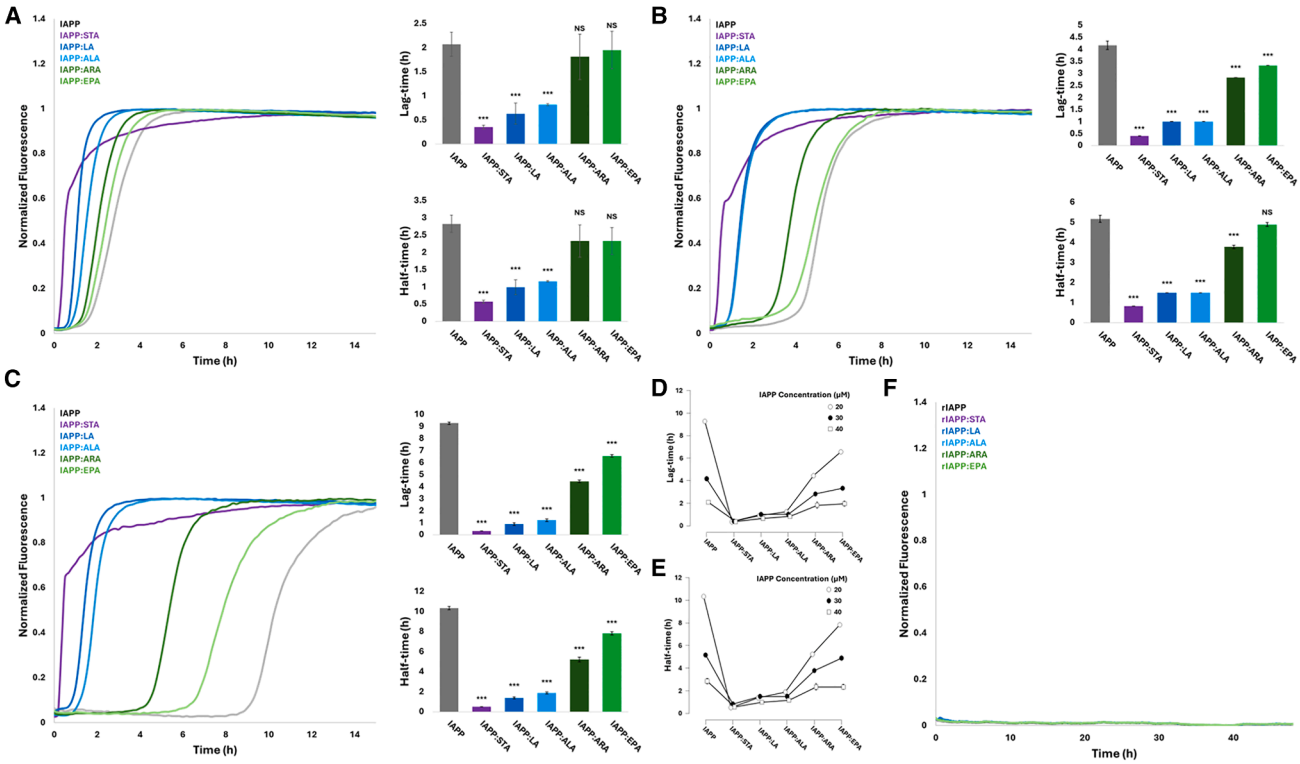

Figure 1. Fatty acids determine the temporal landscape of IAPP aggregation

ThT kinetic curves and quantification of lag-time and half-time for (A) 40 μM, (B) 30 μM, or (C) 20 μM IAPP aggregated in the absence (IAPP) or presence of micelles composed of stearic acid (STA), linoleic acid (LA), alpha linoleic acid (ALA), arachidonic acid (ARA), or eicosapentaenoic acid (EPA). Overlaid line graphs of (D) Lag-time and (E) Half-time values calculated from each set of kinetic experiments. (F) ThT kinetics of nonamyloidogenic rodent IAPP in the absence (rIAPP) or presence of FAs. Bars represent the mean of $N = 3$ individual replicates ± SD. Statistical significance calculated using ANOVA with Tukey's post hoc test. NS = not significant, ***$p < 0.001$.

presence of PUFAs.[25] At the same time, both *n*-3 and *n*-6 FAs lowered the toxicity of $A\beta_{1\text{-}42}$ and transthyretin fibrils.[26,27]

In this study, we utilize Thioflavin T (ThT) kinetic assays to reveal the extent to which different commonly consumed FAs alter the aggregation rate of IAPP. We also employed biophysical techniques to determine the morphology and secondary structure of IAPP:FA aggregates. We further analyzed the relationship between the biophysical properties of IAPP:FA aggregates and their cytotoxicity to pancreatic β-cells and dopaminergic neurons. Finally, *Caenorhabditis elegans* that overexpress IAPP were used to test if FA-induced changes in nematode diet could alter the lifespan of these model organisms.

RESULTS

Length and saturation of fatty acids determine the aggregation rate of islet amyloid polypeptide

To reveal the role of length, saturation, and omega double bond location of FAs on IAPP aggregation, we incubated the monomeric protein in a lipid-free environment and the presence of fatty acid micelles composed of stearic acid (STA, 18:0), linoleic acid (LA, 18:2*n*-6), α-linoleic acid (ALA, 18:3*n*-3), arachidonic acid (ARA, 20:4*n*-6), and eicosapentaenoic acid (EPA, 20:5*n*-3) at 40 μM IAPP and 400 μM FAs to yield a 1:10 protein:FA ratio (Figure 1A). Under physiological conditions (37°C and pH 7.4) and the lipid free environment, IAPP aggregated with a lag-phase (t_{lag}) of 2.07 h ± 0.25 h. Saturated STA had the greatest accelerating effect on IAPP aggregation, with a significantly shorter t_{lag} of 0.35 h ± 0.04 h. Moreover, Medium chain PUFAs LA and ALA shortened t_{lag} to 0.63 h ± 0.21 h and 0.82 h ± 0.02 h, respectively. On the other hand, long chain PUFAs ARA and EPA had a statistically insignificant accelerating effect on t_{lag} of IAPP aggregation. Further, we observed no relationship between omega double-bond position and lag-time in IAPP aggregation. These results suggest that the accelerating effect of FAs on early stages of IAPP aggregation is dependent upon the length and degree of saturation of the acyl tail but not dependent upon double bond location.

In order to determine if the effects of FAs on IAPP aggregation are IAPP concentration dependent, we performed IAPP concentration-response kinetic experiments at a constant concentration of 400 μM FAs. In a lipid free environment, 30 μM IAPP aggregated with a distinct t_{lag} of 4.17 ± 0.17 h, around double the lag time observed for 40 μM IAPP (Figure 1B). Despite this significant increase in lag time for IAPP in the lipid-free environment, the presence of STA accelerated the lag time to 0.40 ± 0.00 h, comparable to that observed at a higher concentration of IAPP. A similar trend was observed in the presence of medium

chain PUFAs, LA and ALA, with both conditions exhibiting a lag phase of 1.00 ± 0.00 h. Though to a lesser extent, the presence of long-chain PUFAs ARA and EPA significantly accelerated the t_{lag} of 30 μM IAPP (2.83 ± 0.00 and 3.33 ± 0.00 h respectively). The accelerating effects of ARA and EPA micelles were not observed for 40 μM IAPP, indicating that the effects of FAs on IAPP aggregation are IAPP concentration dependent. The effects of FAs on the aggregation kinetics of 20 μM IAPP further emphasized this concentration-dependence (Figure 1C). 20 μM IAPP in the absence of FAs exhibited a value of 9.28 ± 0.09 h, near double that observed at 30 μM and quadruple that observed at 40 μM. Further, STA drastically shortened the t_{lag} of IAPP aggregation to 0.33 ± 0.00 h, comparable to that observed for 30 μM and 40 μM IAPP. A similar trend was observed for IAPP aggregated in the presence of LA and ALA, with a shortened lag-time of 0.89 ± 0.10 h and 1.22 ± 0.09 h respectively. The presence of ARA and EPA, however, exhibited greater accelerating effects on 20 μM IAPP compared to the FA-free environment than those observed for 30 μM and 40 μM IAPP (4.44 ± 0.10 and 6.57 ± 0.10 h, respectively). Together, this suggests that the extent to which FAs accelerate IAPP aggregation is both dependent on the chemical properties of the FAs as well as the concentration of IAPP.

FA micelles exerted similar effects on the rate of 40 μM IAPP fibril elongation (t_{half}) as were observed for t_{lag}. STA enabled the greatest accelerating effect (0.57 h ± 0.09 h) compared to the lipid-free environment (2.83 h ± 0.42 h). Additionally, medium chain PUFAs LA (0.99 h ± 0.19 h) and ALA (1.16 h ± 0.19 h) significantly accelerated t_{half} compared to the FA-free environment, but less significantly than fully saturated STA. We also found that long chain PUFAs ARA and EPA had no significant effect on t_{half} of 40 μM IAPP, which is in good agreement with our observations in the lag-phase of IAPP. Similar effects of medium-chain FAs with high degrees of saturation on t_{half} were observed for 30 μM and 20 μM as well. The presence of STA most significantly accelerated the t_{half} of 30 μM IAPP from 5.17 ± 0.17 h in the FA-free environment to 0.83 ± 0.00 h, while the presence of LA and ALA decreased the half-time to 1.5 ± 0.00 h in both conditions. In good agreement with our observations for t_{lag}, the presence of ARA and EPA accelerated the t_{half} of 30 μM IAPP to 3.78 ± 0.09 h and 4.89 ± 0.10 h, respectively. However, the accelerating effect of EPA was not statistically significant for t_{half}. This indicates that the rate of IAPP fibril elongation is dependent upon both the FA environment and IAPP concentration. This effect is again emphasized by the observed effects of FAs on the half-time of 20 μM IAPP (10.33 ± 0.17 h), with the presence of STA, LA, and ALA exhibiting accelerating effects comparable to those observed for 40 μM and 30 μM IAPP (0.50 ± 0.00, 1.39 ± 0.10, and 1.89 ± 0.10 h, respectively). On the other hand, the accelerating effects of ARA (5.22 ± 0.25 h) and EPA (7.83 ± 0.17 h) were amplified compared to 40 μM IAPP. Additionally, we utilized the nonamyloidogenic rodent isoform of IAPP (rIAPP) as an additional control to confirm that the observed effects of FAs in our kinetic curves indeed resulted from accelerated amyloid formation (Figure 1F). At the highest tested concentration of 40 μM peptide and an identical concentration of 400 μM FAs, rIAPP did not aggregate under physiological conditions after a continuous 48 h of incubation. This demonstrates that FAs specifically accelerate the aggregation of amyloidogenic IAPP, but do not induce aggregation in nonamyloidogenic peptides.

These results indicate that FAs significantly accelerate the aggregation and fibril elongation of IAPP directly dependent upon the length and saturation of the FA, but not the double-bond position. More specifically, the effects of FAs on IAPP aggregation become less prominent as the number of double bonds in the acyl chain increases. Further, FAs with higher degrees of saturation have more consistent accelerating effects on lag-time and half-time across multiple IAPP concentrations, while the accelerating effects of long-chain PUFAs with lower degrees of saturation exhibit an IAPP concentration-dependence (Figures 1D and 1E). These observed effects are also specific to amyloidogenic IAPP and do not apply to the aggregation of nonamyloidogenic peptides. Together, these findings demonstrate that FAs accelerate IAPP aggregation and fibril formation dependent on both the chemical properties of the FAs and the concentration of IAPP, suggesting that cellular FA profiles are of paramount importance across multiple stages of disease progression.

Fatty acids alter the morphology of islet amyloid polypeptide amyloids

We utilized atomic force microscopy (AFM) to visualize and characterize the morphology of IAPP fibrils formed in the presence of FAs or in the lipid-free environment (Figures 2A and 2B). We found that after 48 h of aggregation in the lipid free environment, IAPP formed fibrils that were 6.46 ± 1.4 nm thick. However, we observed that when IAPP fibrils were formed in the presence of STA micelles, much thicker fibrils with an average height of 17.95 ± 5.5 nm were formed. These results indicated that interactions with saturated FAs increase the thickness of IAPP fibrils. We also observed a significant increase in fibril thickness when IAPP was aggregated with PUFAs LA (9.33 ± 2.89 nm), ALA(10.13 ± 2.67 nm), and ARA (9.19 ± 2.47 nm). At the same time, no significant changes in fibril thickness were observed when IAPP was aggregated in the presence of the saturated *n*-3 fatty acid EPA (7.81 ± 1.66 nm). These findings indicate that the presence of fully saturated FAs results in the formation of thicker fibrils compared to the aggregates observed in the presence of PUFAs. We also observed many oligomers present when IAPP was aggregated in the FA-free environment that were not observed in aggregates formed in the presence of FAs. To better quantify the respective oligomeric content with aggregates formed in the presence or absence of FAs, we performed a dot-blot assay utilizing an antibody immunized against amyloid oligomers (Figures 2C and 2D). We observed a drastically higher amount of oligomers formed in the FA-free environment compared to aggregates formed in the presence of FAs. Together, these findings demonstrate that FAs alter IAPP aggregation, templating the formation of a greater amount of thicker fibrils and fewer oligomers compared to IAPP alone.

Fatty acids determine the secondary structure of islet amyloid polypeptide amyloids

We used attenuated total reflectance Fourier transform infrared (ATR-FTIR) spectroscopy to analyze IAPP aggregates formed in the presence of FAs and in the lipid-free environment (Figure 3). In the spectra acquired from all analyzed samples,

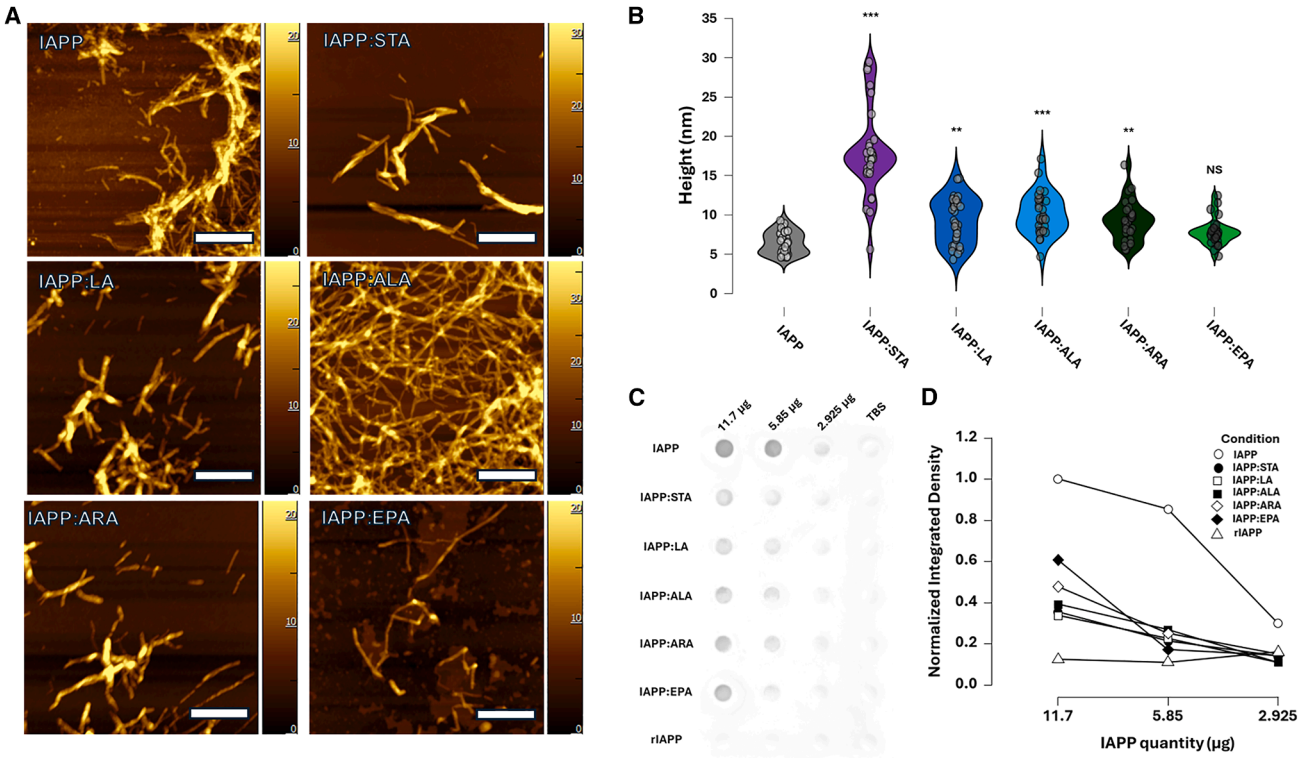

Figure 2. Fatty acids determine the morphology of IAPP amyloids

(A) Representative images of IAPP fibrils grown in the absence of FAs (IAPP) or in the presence of micelles composed of stearic acid (STA), linoleic acid (LA), alpha linoleic acid (ALA), arachidonic acid (ARA), or eicosapentaenoic acid (EPA). Scale bars = 500 nm. (B) Violin plots of height profiles from $N = 30$ fibrils grown in the presence or absence of FAs. (C) A11 dot-blot and (D) quantification of IAPP oligomers. Significance calculated using ANOVA with Tukey's Post Hoc Test. NS = not significant, $^{**}p < 0.01$, $^{***}p < 0.001$.

we found a sharp peak at 1630 cm^{-1}, indicating the predominance of parallel β-sheet. A shoulder centered at 1694 cm^{-1} was also observed in the spectra collected from all samples, indicating that IAPP aggregates have some amount of anti-parallel β-sheet. We also observe a peak at 1660 cm^{-1}, which corresponds to α-helical, random coiling, and β-turn secondary structure. This peak was much more intense in the spectra collected from samples incubated with PUFAS and in the FA-free environment, while 1630 cm^{-1} peak was more prominent in the spectra acquired from IAPP:STA. This suggests that saturated FAs facilitate the formation of parallel β-sheet, while PUFAs promote the formation of α-helical, random coiling, and β-turn as well as parallel β-sheet secondary structure. At the same time, an intense 1660 cm^{-1} band indicates the presence of unaggregated protein and amorphous aggregates in the analyzed samples. To avoid the possible contribution of these populations to the spectroscopic signature of IAPP amyloids, we used atomic force microscopy infrared (AFM-IR) spectroscopy to resolve secondary structure specifically in amyloid fibrils. In AFM-IR, samples deposited on gold-coated silicon substrates can be analyzed using metallized scanning probes.[28,29] Once the sample topology is revealed, the scanning probe can be localized to a specific fibril and illuminated by a pulsed tunable IR source.[30–32] This IR source causes photothermal expansions in the sample, which, in turn, are detected by the change in oscillation frequency of the scanning probe.[33–35] Deconvolution of the frequency changes provides the IR spectra, which can be used to interpret the secondary structure of the analyzed samples.[36,37]

AFM-IR analysis revealed that IAPP fibrils formed in the presence and absence of FAs have predominantly β-sheet secondary structure (Figures 4A and 4B). We found that the amount of parallel β-sheet was considerably smaller in all analyzed aggregates compared to anti-parallel β-sheet. We observed 21.99 ± 6.24% of parallel β-sheet, 25.37 ± 8.3% α-helix, random coiling, and β-turns, and 52.64 ± 5.23% anti-parallel β-sheet in IAPP fibrils formed in the lipid-free environment. IAPP fibrils formed in the presence of STA had a significantly higher amount of anti-parallel β-sheet (78.76 ± 4.59%) and lower amounts of parallel β-sheet (8.98 ± 0.84%) and α-helix, random coiling, and β-turn content (12.26 ± 3.76%). On the other hand, fibrils formed in the presence of PUFAs ALA, ARA, and EPA had very similar, if not identical, secondary structure to IAPP fibrils formed in the lipid-free environment. Finally, we found that in the presence of LA, IAPP formed fibrils with significantly less helix, random coiling, and β-turn content (8.73 ± 1.02%) and significantly higher amount of parallel β-sheet (35.83 ± 2.66%) compared to fibrils grown in the absence of other PUFAs. Moreover, a 1730 cm^{-1} band was present in all AFM-IR spectra of fibrils grown in the presence of PUFAs, but not STA. These results indicate that FAs uniquely alter the secondary structure of IAPP fibrils through protein-FA

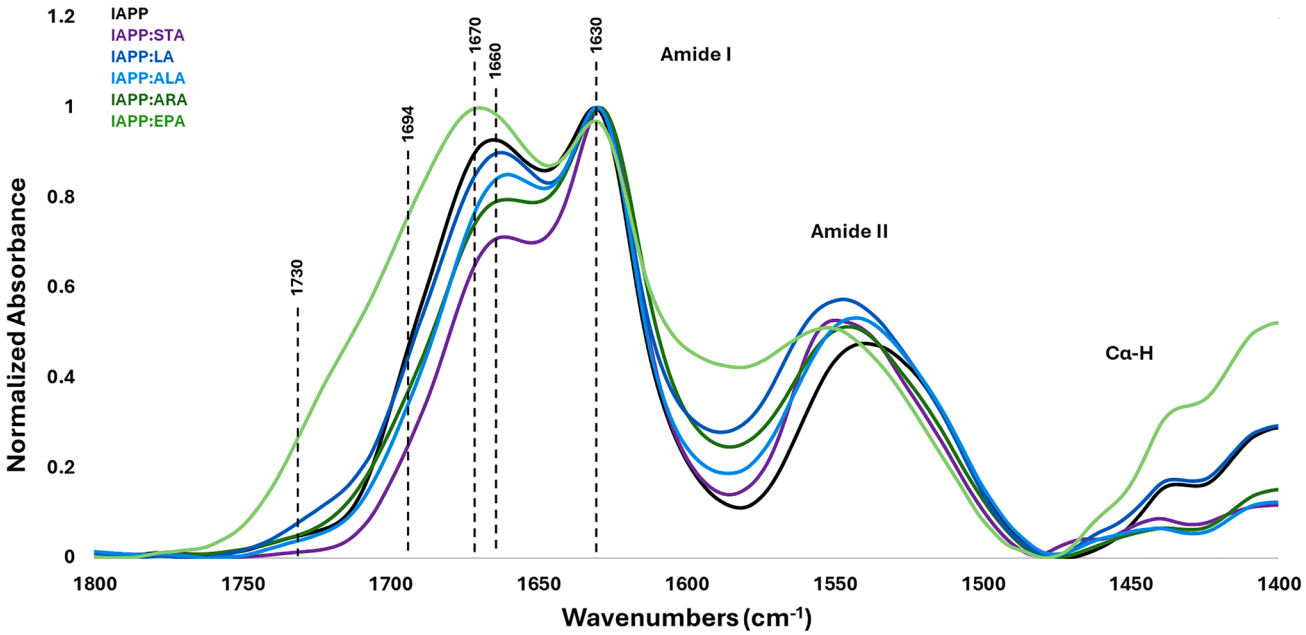

Figure 3. Fatty acids determine the secondary structure of IAPP aggregates

Normalized ATR-FTIR spectra of IAPP aggregates grown in the presence or absence of micelles composed of stearic acid (STA), linoleic acid (LA), alpha linoleic acid (ALA), arachidonic acid (ARA), or eicosapentaenoic acid (EPA). Spectra are coaverages of $N = 3$ spectra.

interaction. Furthermore, saturated FAs and FAs with a low amount of double bonds exerted the greatest impact on the secondary structure of fibrils compared to PUFAs.

Fatty acids determine the toxicity of islet amyloid polypeptide amyloids

To better understand the cellular effects of IAPP:FA aggregates in pancreatic β cells, we utilized fluorescent based flow cytometry assays to determine the toxicity of IAPP aggregates formed in the presence and absence of FAs. Cell-ROX deep red assay was used to quantify the amount of reactive oxygen species (ROS) present in BRIN-BD11 pancreatic β-cells exposed to IAPP:FA aggregates. We observed a significant increase in cytoplasmic ROS levels in pancreatic β cells exposed to 12 μM of IAPP aggregates formed in the absence of FAs (22.75 ± 1.21%) compared to the vehicle control (6.93 ± 1.10%) (Figure 5A). IAPP aggregates formed in the presence of STA were more toxic (31.95 ± 1.35%) compared to those formed in the absence of FAs, indicating that saturated FAs increase the toxicity of IAPP aggregates. We observed an even more significant increase in ROS levels elicited by IAPP aggregates formed in the presence of *n*-6 FAs, LA, and ARA (32.2 ± 1.21% and 35.75 ± 1.40% respectively). Moreover, cells exposed to IAPP aggregates grown in the presence of *n*-3 FAs, ALA and EPA both yielded higher ROS compared to those formed in a FA-free environment (28.35 ± 1.25% and 28.2 ± 0.75% respectively). However, these ROS levels were lower than those observed for *n*-6 FAs and similar to those found for IAPP:STA. These results indicate that FAs uniquely alter the cytotoxic ROS levels elicited by IAPP aggregates based upon the chemical properties of the FAs present during aggregation. We also observed minimal differences between long-chain FAs and medium-chain FAs with the same omega double-bond position, suggesting that the length of the fatty acyl chain contributes less than the omega double-bond position and saturation of the fatty acyl chain to the toxic effects exerted onto pancreatic β cells by IAPP:FA aggregates.

Building upon these findings, we assessed the extent to which the elicited cytotoxic effects of IAPP:FA aggregates are dependent upon IAPP concentration. Decreasing the delivered concentration of IAPP to 9 μM or 6 μM decreased the ROS levels of β cells to 18.37 ± 0.78% and 14.47 ± 1.10%, respectively, when aggregates were formed in the FA-free environment (Figures 5B and 5C). Consistent with what was observed previously, the presence of STA during aggregation significantly increased the elicited ROS levels in β cells exposed to the formed aggregates compared to the FA-free environment at the same concentration of IAPP (23.13 ± 1.07% and 17.50 ± 0.70% respectively). This suggests that the presence of saturated FAs during IAPP aggregation increases the toxicity of IAPP aggregates independent of IAPP concentration. We also observed similar trends for IAPP:PUFA aggregates, as was observed for conditions containing 12 μM IAPP. IAPP aggregated in the presence of *n*-6 PUFAs LA (27.37 ± 1.36% and 20.70 ± 1.85% respectively) and ARA (25.70 ± 0.90 and 20.30 ± 0.10% respectively) resulted in aggregates which elicited higher toxicity than IAPP and IAPP:STA aggregates compared to the respective IAPP concentration. Aggregates formed in the presence of *n*-3 PUFAs ALA (23.93 ± 0.41% and 19.60 ± 1.45% respectively), and EPA (20.67 ± 0.55% and 18.07 ± 0.97% respectively) resulted in less cellular ROS than those formed in the presence of *n*-6 PUFAs and more similar to those formed in the presence of STA when the same concentration of IAPP is delivered. These

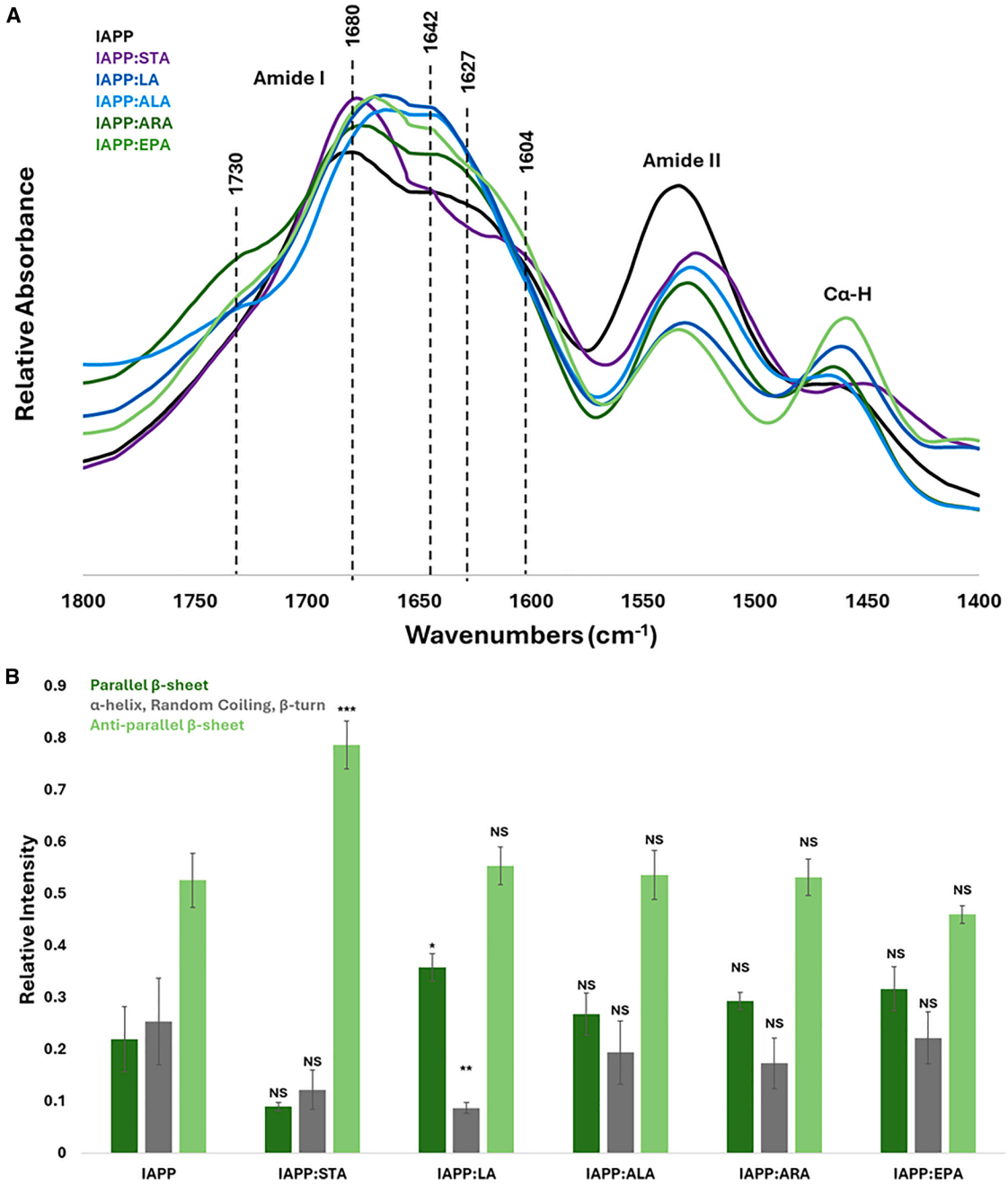

Figure 4. Fatty acids determine the secondary structure of IAPP fibrils

(A) AFM-IR spectra of IAPP fibrils grown in the presence or absence of micelles composed of stearic acid (STA), linoleic acid (LA), alpha linoleic acid (ALA), arachidonic acid (ARA), or eicosapentaenoic acid (EPA). Spectra are coaverages of $N = 30$ spectra.

(B) Quatification results from Gaussian peak fitting of the amide I region of AFM-IR spectra. Plots represent the mean of $n = 30$ spectra ±SD. Significance calculated using ANOVA with Tukey's Post Hoc Test. NS = not significant, $^{*}p < 0.05$, $^{**}p < 0.01$, $^{***}p < 0.001$.

results indicate that the cytotoxic effects of IAPP:FA aggregates are directly dependent on the degree of saturation and omega double-bond position of the FA present during IAPP aggregation but independent of IAPP concentration. Further, while the comparative effects of FAs on IAPP aggregate cytotoxicity are not IAPP concentration dependent, the extent to which IAPP aggregates elicit cytotoxic effects is dependent upon the concentration of IAPP aggregates present (Figure 5D).

In order to determine if the observed cytotoxic effects were due to general FA toxicity, we performed dose response CellROX deep red assays in pancreatic β cells with the individual FAs in the absence of IAPP (Figure 5E). Maintaining the same

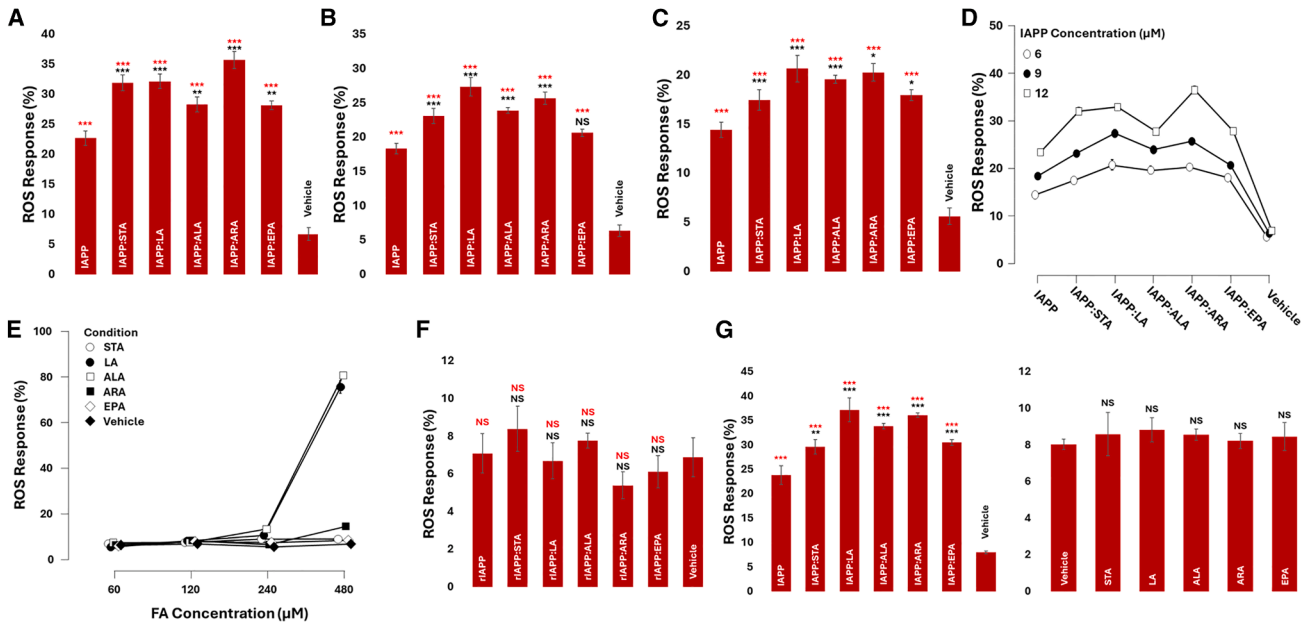

Figure 5. Fatty acids alter the toxicity of IAPP fibrils and ROS levels exerted by these aggregates in pancreatic cells and neurons

ROS levels in BRIN-BD11 pancreatic β cells resulting from exposure to (A) 12 μM, (B) 9 μM, or (C) 6 μM IAPP aggregates grown in the absence (IAPP) or presence of micelles composed of stearic acid (STA), linoleic acid (LA), alpha linoleic acid (ALA), arachidonic acid (ARA), or eicosapentaenoic acid (EPA).

(D) Overlaid line plot of ROS levels at each tested concentration of IAPP.

(E) Dose response ROS levels in BRIN-BD11 pancreatic β cells treated with FAs only.

(F) ROS levels of BRIN-BD11 pancreatic β cells treated with rodent IAPP incubated in the absence or presence of FAs.

(G) ROS levels of N27 neurons treated with IAPP aggregated in the presence or absence of FAs (left panel) or FAs alone (right panel). Bars represent the mean of $N = 3$ independent cultures ± SD. Significance calculated using ANOVA with Tukey's Post Hoc test. Red asterisks represent significance compared to the vehicle control, and black asterisks represent significance against IAPP alone. NS = not significant, $^{**}p < 0.01$, $^{***}p < 0.001$.

120 μM concentration of delivered FAs, we observed no significant differences between ROS levels in β cells exposed to FAs and those exposed to the vehicle control. Doubling the concentration of FAs to 240 μM resulted in a significant increase in ROS levels only for ALA (13.4 ± 1.36%) when compared to the vehicle control (6.90 ± 1.04%). However, the observed increase in cytotoxicity was significantly less than that observed for any condition containing IAPP. When the delivered concentration of FAs was quadrupled, we observed a drastic increase in cytotoxic effects for LA (75.57 ± 4.66%) and ALA (80.8 ± 1.25%), with a less significant increase in toxicity from ARA (14.57 ± 1.10%). No significant increase in toxicity was observed for STA and EPA at any concentration tested. Together, these findings indicate that FAs can be toxic at high concentrations; however, the observed cytotoxic effects of IAPP:FA aggregates did not result from the FAs present. We also tested the effects of nonamyloidogenic rIAPP incubated in the presence of FAs in β cells to determine if general proteotoxicity in combination with FA influx could contribute to the observed cytotoxic effects (Figure 5F). rIAPP:FA treatment resulted in no significant difference in ROS levels compared to the vehicle control. Together, these results demonstrate that the elicited cytotoxicity results from IAPP:FA amyloids, with FAs alone and nonamyloid proteins having minimal, if any effect.

To assess the tissue specificity of IAPP:FA aggregate toxicity, we further performed CellROX deep red assays in N27 dopaminergic neurons (Figure 5G). Delivering FA-free IAPP aggregates at the highest concentration tested for β cells resulted in 23.87 ± 1.88% ROS in neurons, significantly higher than the vehicle control (8.03 ± 0.29%) and similar to that observed in β cells. The presence of saturated STA during aggregation significantly increased the produced aggregate toxicity to 29.67 ± 1.47%, comparable to the effects observed on β cells. The most significant increase in ROS levels, however, resulted from aggregates grown in the presence *n*-6 PUFAs LA (37.23 ± 2.47%) and ARA (36.13 ± 0.46%). On the other hand, aggregates grown in the presence of *n*-3 PUFAs ALA and EPA elicited similar cytotoxic effects as those grown in the presence of STA (33.87 ± 0.58% and 30.53 ± 0.59% respectively). The observed effects of individual FAs on IAPP aggregate toxicity are similar in both neurons and β cells, indicating the cellular effects of IAPP aggregates are not tissue specific. Further, the FA-dependent effects of IAPP:FA aggregates across multiple tissues suggest that there is a conserved mechanism of toxicity elicited by IAPP:FA aggregates.

As mitochondrial dysfunction has been linked to increased cellular ROS and the progression of amyloid diseases,[38–40] we assessed the extent to which IAPP:FA aggregates damage mitochondria in β cells and neurons utilizing the JC-1 assay (Figures 6A and 6B). In the JC-1 assay, flow cytometry is used to quantify green fluorescence in the cells that originates from depolarized mitochondria. Exposure to IAPP aggregates formed in the absence of FAs induced an observed 24.37 ± 1.36% JC-1

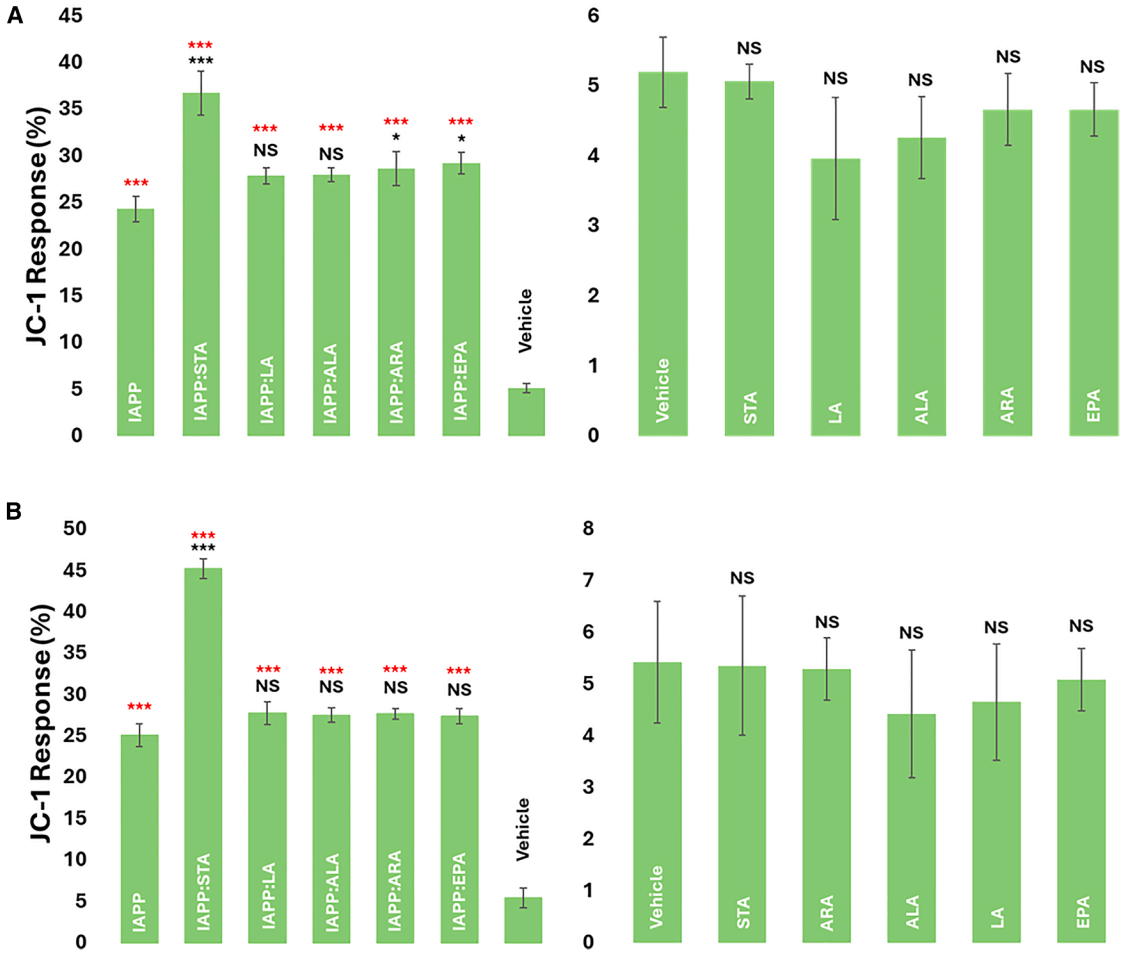

Figure 6. Fatty acids alter the extent to which IAPP fibrils impair mitochondria in pancreatic cells and neurons

JC-1 intensity in BRIN-BD11 pancreatic β cells (A) and N27 neurons (B) exposed to IAPP aggregates (left-hand panels) grown in the presence or absence of micelles composed of stearic acid (STA), linoleic acid (LA), alpha linoleic acid (ALA), arachidonic acid (ARA), or eicosapentaenoic acid (EPA), as well as FAs themselves (righ-hand panels). Bars represent the mean of $N = 3$ independent cultures ± SD. Significance calculated using ANOVA with Tukey's Post Hoc Test. Red asterisks represent significance against the vehicle control, black asterisks represent significance against IAPP alone. NS = not significant, $^{*}p < 0.05$, $^{***}p < 0.001$.

response in pancreatic β cells and 25.17 ± 1.38% in dopaminergic neurons. JC-1 intensity significantly increased in pancreatic β cells (36.77 ± 2.38%) and neurons (45.27 ± 1.17%) exposed to IAPP:STA aggregates. These results indicate that saturated FAs modify IAPP aggregates in a way that increases their damage to mitochondrial membranes. We also observed a much less significant increase in JC-1 response in pancreatic cells for IAPP aggregates that were grown in the presence of long chain PUFAs. Specifically, IAPP:ARA and IAPP:EPA aggregate exposure caused 28.7 ± 1.83% and 29.23 ± 1.16% mitochondrial depolarization, respectively. However, neurons exposed to IAPP aggregates grown in the presence of long-chain PUFAS caused no significant difference in mitochondrial depolarization compared to the FA free environment. Furthermore, no significant change in JC-1 response for IAPP aggregates formed in the presence of medium chain PUFAs LA and ALA was observed in either cell line, suggesting that mitochondrial damage caused by IAPP amyloids is most dependent on fatty acyl saturation. Together, the observed trends across cell lines for the JC-1 assay suggest that mitochondrial damage caused by IAPP aggregates grown in the presence of FAs can be tuned in a saturation dependent manner. However, the mitochondrial damage is most dependent on the degree of saturation of the FA tail, not the omega double-bond location. Further, these results suggest that mitochondrial damage is not the sole source of ROS observed in cells exposed to IAPP:FA, independent of tissue type.

Fatty acids alter the transcriptional response in pancreatic β cells and neurons

To further analyze cellular responses in the cells exposed to IAPP fibrils formed in the presence or absence of FAs, we determined changes in the expression of genes responsible for unfolded protein response (UPR), exosome secretion, mitophagy, and autophagy in β cells (Figure 7). We found that ATF6 expression, a key protein in endoplasmic reticulum (ER) UPR, was on average

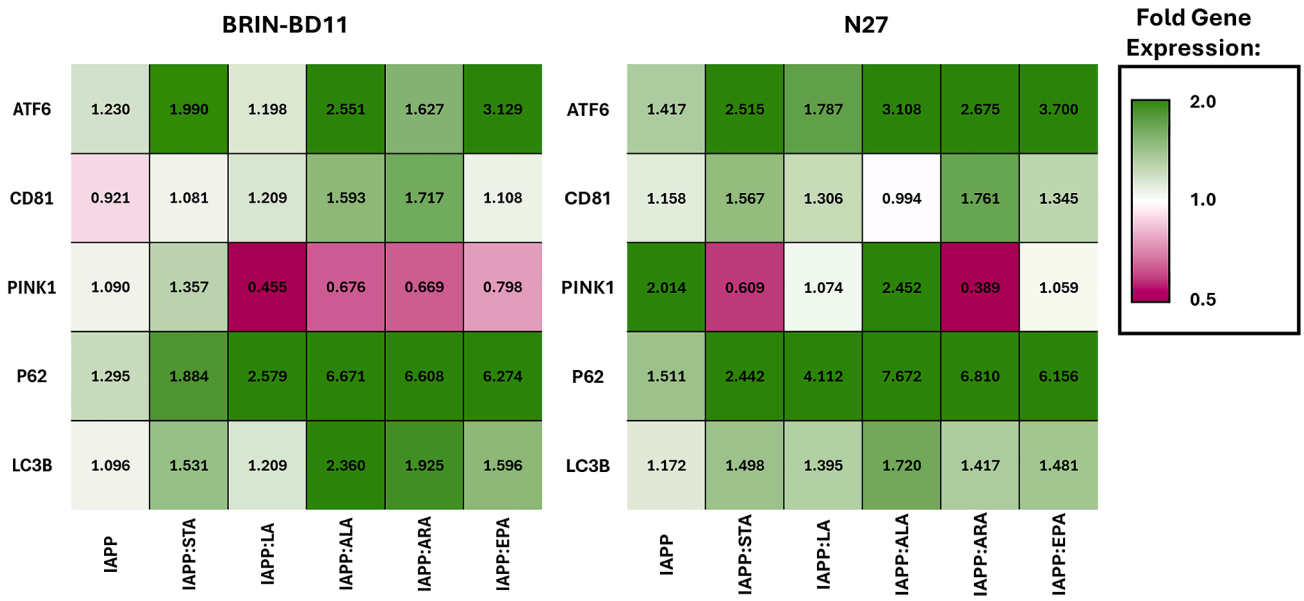

Figure 7. Fatty acids determine transcriptional response in pancreatic cells and neurons exposed to IAPP amyloids

RT-qPCR analysis of changes in the expression of ATF6, CD81, PINK1, p62, and LC3B in BRIN-BD11 pancreatic β cells and N27 neurons exposed to IAPP aggregates formed in the presence or absence of micelles composed of stearic acid (STA), linoleic acid (LA), alpha linoleic acid (ALA), arachidonic acid (ARA), or eicosapentaenoic acid (EPA). Plots represent the mean of $N = 3$ replicates.

significantly upregulated in pancreatic cells exposed to IAPP:FA aggregates. Specifically, aggregates formed in the presence of *n*-3 fatty acids ALA and EPA had the highest ATF6 expression in comparison to *n*-6 FAs ARA and LA, as well as saturated STA. This indicates that IAPP:FA aggregates activate UPR in the ER, suggesting the cell's ability to target these aggregates and activate protein quality control machinery is dependent on the FA environment. ER stress and UPR activation have also been shown to contribute to cellular ROS in several amyloid-related diseases, including T2D, suggesting the upregulation of the UPR by IAPP:FA aggregates contributes to increased cellular ROS levels.[41] We also investigated changes in the expression of CD81, a marker of exosome secretion, in pancreatic cells. We observed that the expression was the same or significantly upregulated in pancreatic cells as a result of exposure to IAPP:FA aggregates. This suggests cells exposed to IAPP:FA aggregates may secrete these aggregates in an attempt to reduce toxicity, and this occurs independent of the tissue these aggregates affect. PTEN-induced kinase 1 (PINK1) expression was monitored as a marker of mitophagy, the process by which cells degrade damaged mitochondria. PINK1 expression was downregulated in β cells exposed to IAPP:PUFA aggregates, indicating that cells fail to properly recycle mitochondria damaged by IAPP aggregates. In cells exposed to IAPP:STA aggregates, however, PINK1 is significantly upregulated. This suggests that the role of mitochondria in cellular responses to IAPP:FA aggregates is dependent on the properties of the FA present, consistent with what was observed in our JC-1 assays. We also investigated changes in the expression of P62 and LC3B, markers of cell autophagy. It was found that P62 expression was upregulated in pancreatic cells exposed to IAPP:FA aggregates, with drastically higher expression when aggregates were formed in the presence of PUFAS. LC3B expression, however, was less significantly upregulated. Thus, IAPP:FA aggregates disrupted cell homeostasis once endocytosed by pancreatic β cells, and the extent to which the cell activates detoxifying pathways is dependent upon the properties of the FA present. We additionally tested these transcriptional responses in neurons, where we observed similar transcriptional responses to IAPP:FA aggregates, dependent upon the properties of the FA. Based upon this, our findings also indicate that the saturation of FAs in IAPP:FA aggregates plays a critically important role in the transcriptional activation of both select autophagy genes and the pathway of degradation by which the aggregates are targeted in both β cells and neurons.

Fatty acids determine the toxicity of islet amyloid polypeptide *in vivo*

To test the effects of FA dietary supplementation on the *in vivo* toxicity of IAPP aggregates, we utilized a *C. elegans* DMH46 strain that has been genetically modified to overexpress IAPP when exposed to increased environmental temperatures.[42] We supplemented the worms' normal diet of OP50 E. coli with either STA, LA, or ALA and performed a lifespan assay to compare the relative toxicity of overexpressed IAPP (Figure 8A and Table 1). We observed that supplementation with PUFAs LA and ALA, significantly decreased the median lifespan of the worms (p50 = 11 and 10 days, respectively) when overexpressing IAPP as compared to the worms fed only *E. coli* (p50 = 13 days). We also observed that the supplementation of PUFAs caused worms to begin to die earlier, not just at a faster rate, suggesting these FAs accelerate the onset of the diseased state. STA (p50 = 13), on the other hand, did not affect the lifespan of the diseased worms. In N2 wildtype worms, none of

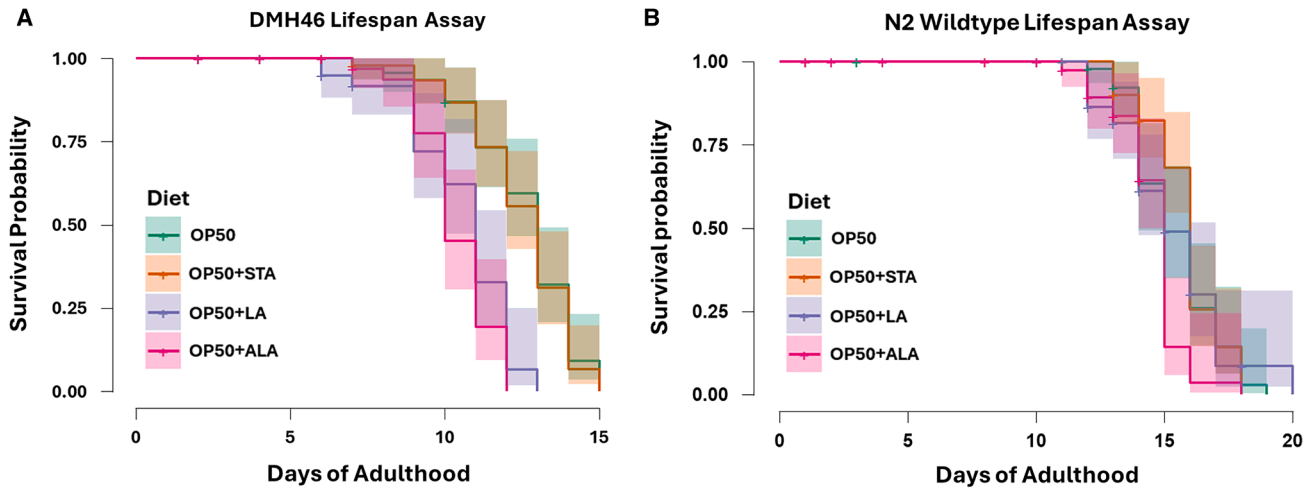

Figure 8. Dietary fatty acids determine the toxicity of IAPP aggregates *in vivo*

Kaplan Meier survival curves with 95% confidence intervals of $N = 50$ DMH46 (A) and N2 (B) *C. elegans* populations with the supplementation of stearic acid (STA), linoleic acid (LA), or alpha linoleic acid (ALA), and without FA supplementation (OP50). Statistical summaries for DMH46 and N2 populations are provided in Tables 1 and 2, respectively. Significance calculated using the Kruskal-Wallis test with Dunn's Post Hoc test.

the FAs significantly affected worm lifespan, with populations supplemented with LA or ALA and worms with no dietary supplementation having a p50 = 15 days, and worms fed diets supplemented with STA having a p50 = 16 days (Figure 8B and Table 2). Together, this suggests that the toxicity of IAPP *in vivo* can be tuned by the dietary lipid profile present, and that the resulting toxicity from dietary supplementation is a result of IAPP overexpression in combination with specific FA enrichment.

DISCUSSION

In this study, we show that FAs have a significant influence on IAPP aggregation, as well as biophysical properties of IAPP fibrils, including their morphology and the secondary structure (Figure 9). We also found that this influence was determined by the length and saturation of FAs. These results are consistent with our previous work in which we demonstrated that the length and saturation of FAs altered aggregation properties of transthyretin.[27] Furthermore, Wilson and co-workers also demonstrated that free FAs in blood serum could facilitate Tau and Aβ aggregation. It was shown that this effect directly depended on the degree of saturation of FAs.[43] Westermark and co-workers found that high serum fatty acid levels led to IAPP overexpression and facilitated protein aggregation, which is in good agreement with our current findings.[44] It is also important to note that free fatty acids in dynamic exchange with membranes or micelles have drastic impacts on amyloid formation, as found by Scollo and coworkers.[45] Thus, we can conclude that free FAs, as well as those within membranes, have a strong influence on IAPP amyloid formation. We further show that the extent to which individual FAs elicit an effect on IAPP aggregation is directly dependent upon the concentration of IAPP present. These findings are consistent with results found by Elenbaas and colleagues, which demonstrated that the extent to which lipid membranes accelerate IAPP aggregation is IAPP-concentration dependent.[9] Further, it has been previously shown by Takada and collaborators that IAPP expression increases with the age and progression of T2D in mice.[46] Together, this suggests that the extent to which cellular FAs affect IAPP aggregation may have implications in the stage of disease progression, with FAs exerting a more prominent effect at the earlier stages of T2D when cellular IAPP concentrations are lower.

We found that all FAs except EPA facilitated the formation of significantly thicker fibrils compared to IAPP alone. STA, specifically, had the most drastic effect, forming fibrils nearly 3-fold thicker on average compared to the IAPP fibrils formed in the absence of lipids. Similar findings were previously reported by our group for transthyretin, α-syn, $A\beta_{1-42}$, and insulin fibrils.[24–27] We further demonstrate that the presence of FAs results in significantly less oligomers during IAPP aggregation. Consistent with what was observed in our kinetic experiments and observations of fibril thickness, the presence of more saturated FAs produced the fewest oligomers. Together, this demonstrates that FAs alter the aggregation of IAPP, which leads to the formation of thicker fibrils that are morphologically distinct from those formed in the FA free environment, as well as the formation of fewer oligomers in accordance with the degree of saturation in the acyl tail. Building upon this, it was also shown by Li and coworkers that IAPP aggregation results in the formation of several polymorphs.[47] AFM-IR analysis showed that IAPP fibrils, regardless of the presence of FAs, had predominantly anti-parallel β-sheet secondary structure. These results are consistent with experimental findings reported by Khemtemourian and co-workers, who found that IAPP fibrils were predominantly composed of antiparallel β-sheet.[48] It was further shown by Roder and colleagues that IAPP fibrils are antiparallel β-sheets, and the structure of these fibrils fits well with the structure of amyloid β fibrils.[49] However, STA caused the most significant difference in the secondary structure of IAPP fibrils. We observed a significantly higher amount of anti-parallel β-sheet structure in IAPP:STA fibrils

Table 1. Statistical analysis of DMH46 *C. elegans*

Dunn's Post Hoc Comparisons – DMH46

Comparison	p_{bonf}	p_{holm}
OP50 - OP50+STA	1.00000	1.00000
OP50 - OP50+LA	7.66578e-7	4.06620e-7
OP50 - OP50+ALA	9.03341e-8	7.52784e-8

Rank-biserial correlation based on individual Mann-Whitney tests.

compared to IAPP alone and IAPP aggregates formed in the presence of PUFAs. This is consistent with what was observed for fibril thickness as well, with the presence of STA leading to much thicker fibrils than those formed in the FA-free environment and in the presence of PUFAs. Our results also show that fibrils formed in the presence of each of the analyzed PUFAs are similar in secondary structure and morphology but differ from those of fibrils formed in the presence of STA and in the absence of FAs. More specifically, the effects of PUFAs on the morphology of IAPP aggregates and oligomeric content were uniquely altered in comparison to IAPP fibrils grown in the FA free environment, but these differences were less significant than those observed in IAPP:STA fibrils. It is also important to note that fibrils grown in the presence of PUFAs had a distinct band around 1730 cm^{-1}, which has been characterized to primarily correspond to the carbonyl in the acyl chain of lipids and FAs.[50,51] However, this band was not present in fibrils grown with STA, or in fibrils grown in the lipid free environment. These findings suggest that PUFAs uniquely template IAPP aggregation, which results in the formation of only certain fibril polymorphs that are coated with or contain FAs, while saturated FAs template fibrils that are more structurally and morphologically distinct. Together, our results demonstrate that the presence of FAs alters the aggregation cascade of IAPP, resulting in the formation of aggregate populations dominated by antiparallel β-sheet rich fibril polymorphs distinct from aggregates formed in the absence of FAs. Further, the saturation of FAs has the most prominent effect on the biophysical properties of IAPP fibrils, with more saturated FAs having the greatest impact on IAPP structure and morphology.

We also found that FAs altered the cytotoxicity of IAPP fibrils, as well as transcriptional responses of pancreatic cells and neurons exposed to these protein aggregates. The JC-1 assay showed that aggregates grown in the presence of STA produced the highest levels of mitochondrial dysfunction compared to IAPP aggregates grown in the FA-free environment and in the presence of PUFAs. This is in good agreement with what was observed for differences in fibril structure and thickness. However, the ROS assay revealed that IAPP aggregates grown in the presence of *n*-6 PUFAs LA and ARA, triggered the most substantial increase in ROS levels compared to IAPP aggregates grown in the absence of FAs or in the presence of STA, ALA, or EPA. These results indicate that FAs alter the molecular mechanisms by which IAPP aggregates cause cytotoxicity. This conclusion is further supported by qPCR analysis of changes in the expression of molecular factors involved in ER UPR, autophagy, and exosome secretion. Specifically, IAPP aggregates formed in the presence of PUFAs caused significantly higher expression of autophagy markers P62 and LC3B, exosome secretion marker CD81, and UPR marker ATF6 in both pancreatic cells and neurons compared to IAPP fibrils grown in the presence of STA or FA-free environment. This suggests that the ability of the cells to target IAPP aggregates and utilize detoxifying machinery to mitigate amyloid toxicity is altered by the FAs present. Further, aggregates formed in the presence of STA triggered an upregulation of mitophagy in β cells, consistent with our results in the JC-1 assay. However, despite eliciting the same degree of mitochondrial damage as the IAPP aggregates formed in the FA-free environment, IAPP:PUFA aggregates led to a downregulation of mitophagy. This indicates that the presence of PUFAs in IAPP aggregates alters mitochondrial dynamics, suggesting that the properties of FAs may alter the role of the mitochondria in amyloid toxicity. Together, these results demonstrate that the mechanism of toxicity elicited by IAPP:FA aggregates is directly dependent on the degree of saturation and double bond location in the FA. Further, this suggests that the FA environment is a modulator of cell toxicity and stress responses in IAPP amyloidosis, bolstering the link between nutritional FA intake and the progression of T2D-related IAPP amyloidosis.

Table 2. Statistical analysis of N2 Wildtype *C. elegans*

Dunn's Post Hoc Comparisons – N2 Wildtype

Comparison	p_{bonf}	p_{holm}
OP50 - OP50+STA	1.00000	0.88778
OP50 - OP50+LA	1.00000	0.88778
OP50 - OP50+ALA	0.15805	0.13171

Rank-biserial correlation based on individual Mann-Whitney tests.

The results of our *C. elegans* experiment further support the potential connection between nutrition and T2D-related IAPP amyloidosis. The supplementation of PUFAs into the nematode diet lowered the median lifespan of worms expressing IAPP, but not wild type worms. This is in good agreement with what was observed for our toxicity assays, suggesting that nutritional lipids alter the cellular effects of IAPP based upon the properties of the FA. Dysfunction in lipid metabolism and high fat diets have also been linked to the pathogenesis and progression of T2D, with the majority of T2D cases exhibiting mixed forms of dyslipidemia.[52] This dyslipidemia has also been associated with higher levels of ROS, mitochondrial dysfunction, ER stress, and dysfunction in autophagy machinery,[53] consistent with what was observed in β cells and neurons. In both worms and cells, differences in toxicity as a consequence of FAs were only observed in the presence of amyloidogenic IAPP and IAPP aggregates. Based upon this, the findings of this study suggest that the effects of IAPP on the progression of T2D are directly linked to dietary and, consequently, cellular FA profiles. This is consistent with work by Ralhan and colleagues in an Alzheimer's model of *Drosophila*. It was demonstrated that lipids and lipid-protein particles can contribute to cell toxicity, and cellular quality control machinery is altered to clear these toxic particles and prevent cell death.[54] Thus, we conclude that the progression and consequence of T2D-related IAPP amyloidosis is determined by both the properties of the IAPP amyloids formed in the cellular environment as well as the cellular FA profile.

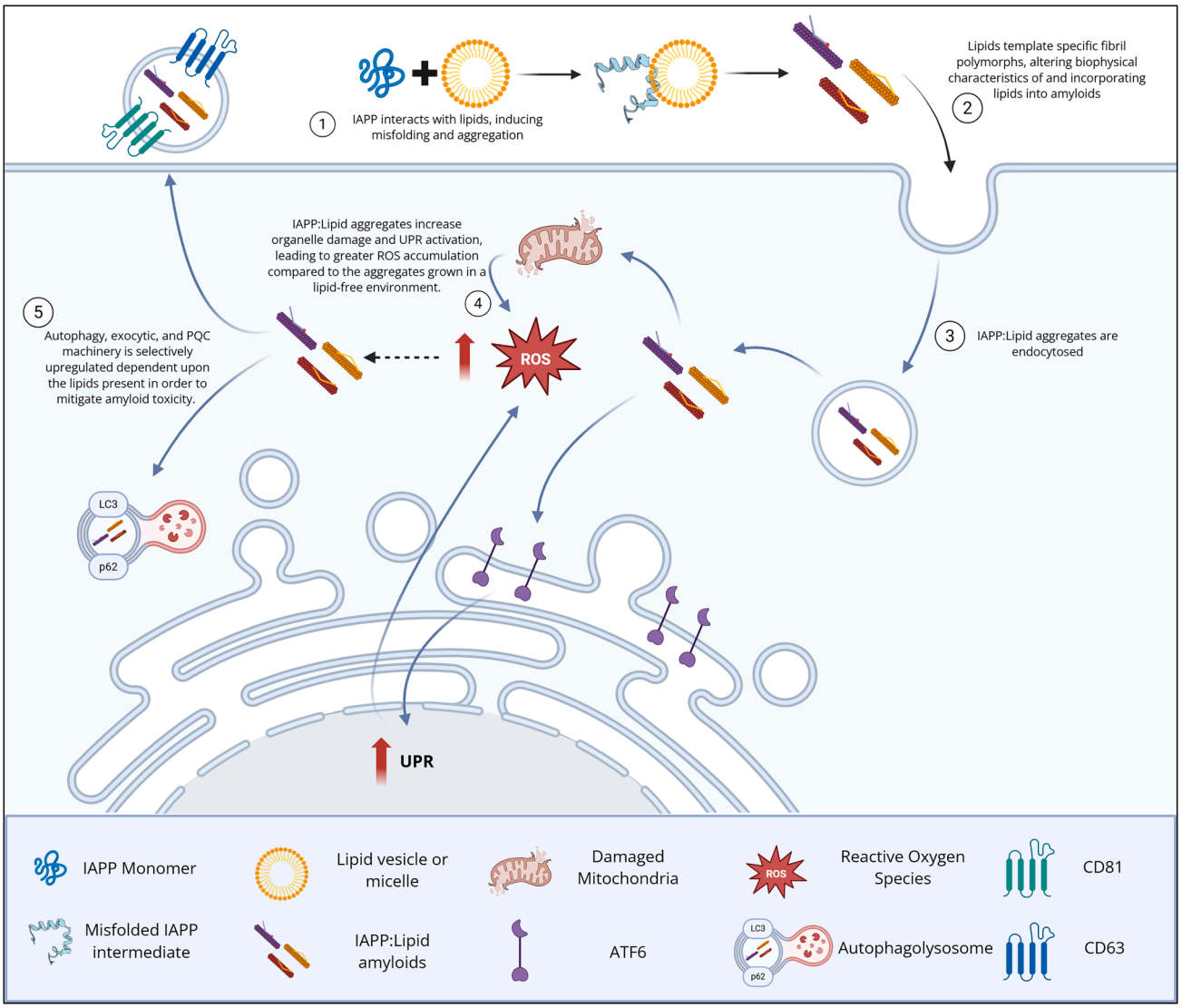

Figure 9. Proposed model by which FAs determine the toxicity of IAPP amyloids

Together, the results of this study demonstrate the importance of FAs, an essential class of nutritional lipids, in the development and progression of T2D related IAPP amyloidosis, and indicate the need for a deeper understanding of the crosstalk between nutrition, lipid metabolism, and amyloid aggregation.

Summarizing, we can conclude that FAs alter the aggregation properties of IAPP, accelerating the aggregation of IAPP and facilitating the formation of unique aggregate populations. Furthermore, the presence of FAs at the beginning stage of protein aggregation resulted in the formation of structurally and morphologically different IAPP fibril polymorphs compared to those grown in the lipid-free environment. These differences between polymorphs changed the cytotoxicity of IAPP aggregates, altering the target and mechanism of cytotoxicity. Our results also indicate that FAs alter molecular mechanisms by which β cells and neurons respond to IAPP aggregates and their exerted cytotoxic effects. Finally, *C. elegans* lifespan assays demonstrate that the toxic consequence of IAPP *in vivo* is directly dependent upon profiles of consumed FAs. These results suggest that nutritional FAs may play a very important role in the onset and progression of T2D, and that amyloids and lipids contribute synergistically to β cell toxicity. Furthermore, drug candidates that disrupt lipid-IAPP interactions, consequently decelerating IAPP aggregation, may improve current therapeutic strategies for T2D.

Limitations of the study

The current study is primarily limited by the use of BRIN-BD11 hybridoma cells that do not fully encapsulate β cell physiology. Consequently, additional validation of the reported results on primary cells is highly important to fully understand the role of lipids in the IAPP-driven T2D. Furthermore, studies focused on molecular and genetic pathways in the *C. elegans* that overexpress IAPP would provide important insight into the *in vivo*

mechanisms of IAPP-driven toxicity. Finally, the utilization of higher order vertebrates as models of T2D will be important metabolic processes that do not occur in nematodes but exist in mammals. This would be even further bolstered by the investigation of IAPP aggregation and turnover within the model organism, which will be a focus of future studies.

RESOURCE AVAILABILITY

Lead contact

Further information and requests for resources should be directed to the lead contact, Dmitry Kurouski (dkurouski@tamu.edu).

Materials availability

This study did not generate new unique reagents. All material generated during this study are available from the lead contact upon request.

Data and code availability

- Data: All data generated or analyzed during this study are available from the lead contact upon request.
- Code: This study did not generate any new code.
- For all other information and requests, please submit inquiries to the lead contact, Dmitry Kurouski (dkurouski@tamu.edu)

ACKNOWLEDGMENTS

We are grateful to the National Institutes of Health for the provided financial support (R35GM142869).

AUTHOR CONTRIBUTIONS

J.S. – conceptualization, investigation, visualization, data analysis, and writing original article and editing; D.P., A.H., and Ro.E. – investigation; D.K. – supervision, resources, project administration, and funding acquisition.

DECLARATION OF INTERESTS

The authors declare no conflicts of interest.

STAR★METHODS

Detailed methods are provided in the online version of this paper and include the following:

- KEY RESOURCES TABLE
- EXPERIMENTAL MODELS AND STUDY PARTICIPANT DETAILS
  - Cell culture
  - Caenorhabditis elegans
- METHOD DETAILS
  - Fatty acid micelle preparation
  - Protein sourcing and preparation
  - Thioflavin T (ThT) kinetics
  - Atomic force microscopy (AFM)
  - A11 dot-blot analysis
  - Attenuated total reflectance Fourier transform infrared (ATR-FTIR) spectroscopy
  - Nano-IR spectroscopy
  - Cell toxicity assays
  - Real time quantitative PCR (qPCR)
  - Caenorhabditis elegans
- QUANTIFICATION AND STATISTICAL ANALYSIS

Received: April 29, 2025
Revised: August 30, 2025
Accepted: December 5, 2025
Published: December 10, 2025

REFERENCES

1. Ye, J., Wu, Y., Yang, S., Zhu, D., Chen, F., Chen, J., Ji, X., and Hou, K. (2023). The global, regional and national burden of type 2 diabetes mellitus in the past, present and future: a systematic analysis of the Global Burden of Disease Study 2019. Front. Endocrinol. *14*, 1192629. https://doi.org/10.3389/fendo.2023.1192629.
2. GBD 2021 Diabetes Collaborators (2023). Global, regional, and national burden of diabetes from 1990 to 2021, with projections of prevalence to 2050: a systematic analysis for the Global Burden of Disease Study 2021. Lancet *402*, 203–234. https://doi.org/10.1016/S0140-6736(23)01301-6.
3. Akter, R., Cao, P., Noor, H., Ridgway, Z., Tu, L.H., Wang, H., Wong, A.G., Zhang, X., Abedini, A., Schmidt, A.M., and Raleigh, D.P. (2016). Islet Amyloid Polypeptide: Structure, Function, and Pathophysiology. J. Diabetes Res. *2016*, 2798269. https://doi.org/10.1155/2016/2798269.
4. Hassan, S., White, K., and Terry, C. (2022). Linking hIAPP misfolding and aggregation with type 2 diabetes mellitus: a structural perspective. Biosci. Rep. *42*, BSR20211297. https://doi.org/10.1042/BSR20211297.
5. Westermark, P., Andersson, A., and Westermark, G.T. (2011). Islet amyloid polypeptide, islet amyloid, and diabetes mellitus. Physiol. Rev. *91*, 795–826. https://doi.org/10.1152/physrev.00042.2009.
6. Alrouji, M., Al-Kuraishy, H.M., Al-Gareeb, A.I., Alexiou, A., Papadakis, M., Saad, H.M., and Batiha, G.E.S. (2023). The potential role of human islet amyloid polypeptide in type 2 diabetes mellitus and Alzheimer's diseases. Metab. Syndr. *15*, 101. https://doi.org/10.1186/s13098-023-01082-1.
7. Bharadwaj, P., Solomon, T., Sahoo, B.R., Ignasiak, K., Gaskin, S., Rowles, J., Verdile, G., Howard, M.J., Bond, C.S., Ramamoorthy, A., et al. (2020). Amylin and beta amyloid proteins interact to form amorphous heterocomplexes with enhanced toxicity in neuronal cells. Sci. Rep. *10*, 10356. https://doi.org/10.1038/s41598-020-66602-9.
8. Milardi, D., Gazit, E., Radford, S.E., Xu, Y., Gallardo, R.U., Caflisch, A., Westermark, G.T., Westermark, P., Rosa, C.L., and Ramamoorthy, A. (2021). Proteostasis of Islet Amyloid Polypeptide: A Molecular Perspective of Risk Factors and Protective Strategies for Type II Diabetes. Chem. Rev. *121*, 1845–1893. https://doi.org/10.1021/acs.chemrev.0c00981.
9. Elenbaas, B.O.W., Khemtemourian, L., Killian, J.A., and Sinnige, T. (2022). Membrane-Catalyzed Aggregation of Islet Amyloid Polypeptide Is Dominated by Secondary Nucleation. Biochemistry *61*, 1465–1472. https://doi.org/10.1021/acs.biochem.2c00184.
10. Mo, X.D., Gao, L.P., Wang, Q.J., Yin, J., and Jing, Y.H. (2018). Lipid accelerating the fibril of islet amyloid polypeptide aggravated the pancreatic islet injury in vitro and in vivo. Lipids Health Dis. *17*, 42. https://doi.org/10.1186/s12944-018-0694-8.
11. Zhang, X., St Clair, J.R., London, E., and Raleigh, D.P. (2017). Islet Amyloid Polypeptide Membrane Interactions: Effects of Membrane Composition. Biochemistry *56*, 376–390. https://doi.org/10.1021/acs.biochem.6b01016.
12. Nanga, R.P.R., Brender, J.R., Vivekanandan, S., and Ramamoorthy, A. (2011). Structure and membrane orientation of IAPP in its natively amidated form at physiological pH in a membrane environment. Biochim. Biophys. Acta *1808*, 2337–2342. https://doi.org/10.1016/j.bbamem.2011.06.012.
13. Ma, Z., and Westermark, G.T. (2002). Effects of free fatty acid on polymerization of islet amyloid polypeptide (IAPP) in vitro and on amyloid fibril formation in cultivated isolated islets of transgenic mice overexpressing human IAPP. Mol. Med. *8*, 863–868.
14. Pallbo, J., Olsson, U., and Sparr, E. (2021). Strong inhibition of peptide amyloid formation by a fatty acid. Biophys. J. *120*, 4536–4546. https://doi.org/10.1016/j.bpj.2021.08.035.
15. Lopez, S., Bermudez, B., Ortega, A., Varela, L.M., Pacheco, Y.M., Villar, J., Abia, R., and Muriana, F.J.G. (2011). Effects of meals rich in either monounsaturated or saturated fat on lipid concentrations and on insulin secretion and action in subjects with high fasting triglyceride

concentrations. Am. J. Clin. Nutr. *93*, 494–499. https://doi.org/10.3945/ajcn.110.003251.

16. Avallone, R., Vitale, G., and Bertolotti, M. (2019). Omega-3 Fatty Acids and Neurodegenerative Diseases: New Evidence in Clinical Trials. Int. J. Mol. Sci. *20*, 4256. https://doi.org/10.3390/ijms20174256.
17. Fiala, M., Lau, Y.C.C., Aghajani, A., Bhargava, S., Aminpour, E., Kaczor-Urbanowicz, K.E., Mirzoyan, H., Nichols, I., Ko, M.W., Morselli, M., et al. (2020). Omega-3 Fatty Acids Increase Amyloid-beta Immunity, Energy, and Circadian Rhythm for Cognitive Protection of Alzheimer's Disease Patients Beyond Cholinesterase Inhibitors. J. Alzheimers Dis. *75*, 993–1002. https://doi.org/10.3233/JAD-200252.
18. Dighriri, I.M., Alsubaie, A.M., Hakami, F.M., Hamithi, D.M., Alshekh, M.M., Khobrani, F.A., Dalak, F.E., Hakami, A.A., Alsueaadi, E.H., Alsaawi, L.S., et al. (2022). Effects of Omega-3 Polyunsaturated Fatty Acids on Brain Functions: A Systematic Review. Cureus *14*, e30091. https://doi.org/10.7759/cureus.30091.
19. Prada, M., Eichelmann, F., Wittenbecher, C., Kuxhaus, O., and Schulze, M.B. (2023). Plasma Lipidomic n-6 Polyunsaturated Fatty Acids and Type 2 Diabetes Risk in the EPIC-Potsdam Prospective Cohort Study. Diabetes Care *46*, 836–844. https://doi.org/10.2337/dc22-1435.
20. Wu, J.H.Y., Marklund, M., Imamura, F., Tintle, N., Ardisson Korat, A.V., de Goede, J., Zhou, X., Yang, W.S., de Oliveira Otto, M.C., Kröger, J., et al. (2017). Omega-6 fatty acid biomarkers and incident type 2 diabetes: pooled analysis of individual-level data for 39 740 adults from 20 prospective cohort studies. Lancet Diabetes Endocrinol. *5*, 965–974. https://doi.org/10.1016/S2213-8587(17)30307-8.
21. Taha, A.Y. (2020). Linoleic acid-good or bad for the brain? NPJ Sci. Food *4*, 1. https://doi.org/10.1038/s41538-019-0061-9.
22. Mercola, J., and D'Adamo, C.R. (2023). Linoleic Acid: A Narrative Review of the Effects of Increased Intake in the Standard American Diet and Associations with Chronic Disease. Nutrients *15*, 3129. https://doi.org/10.3390/nu15143129.
23. Wijendran, V., and Hayes, K.C. (2004). Dietary n-6 and n-3 fatty acid balance and cardiovascular health. Annu. Rev. Nutr. *24*, 597–615. https://doi.org/10.1146/annurev.nutr.24.012003.132106.
24. Hoover, Z., Lynn, M., Zhaliazka, K., Holman, A.P., Dou, T., and Kurouski, D. (2024). Long-Chain Polyunsaturated Fatty Acids Accelerate the Rate of Insulin Aggregation and Enhance Toxicity of Insulin Aggregates. ACS Chem. Neurosci. *15*, 147–154. https://doi.org/10.1021/acschemneuro.3c00583.
25. Ali, A., Holman, A.P., Rodriguez, A., Osborne, L., and Kurouski, D. (2024). Elucidating the mechanisms of alpha-Synuclein-lipid interactions using site-directed mutagenesis. Neurobiol. Dis. *198*, 106553. https://doi.org/10.1016/j.nbd.2024.106553.
26. Zhaliazka, K., and Kurouski, D. (2024). Nanoscale Structural Characterization of Amyloid beta 1-42 Oligomers and Fibrils Grown in the Presence of Fatty Acids. ACS Chem. Neurosci. *15*, 3344–3353. https://doi.org/10.1021/acschemneuro.4c00275.
27. Ali, A., Zhaliazka, K., Dou, T., Holman, A.P., and Kurouski, D. (2023). Saturation of fatty acids in phosphatidic acid uniquely alters transthyretin stability changing morphology and toxicity of amyloid fibrils. Chem. Phys. Lipids *257*, 105350. https://doi.org/10.1016/j.chemphyslip.2023.105350.
28. Dazzi, A., Glotin, F., and Carminati, R. (2010). Theory of infrared nanospectroscopy by photothermal induced resonance. J. Appl. Phys. *107*, 124519.
29. Dazzi, A., and Prater, C.B. (2017). AFM-IR: Technology and Applications in Nanoscale Infrared Spectroscopy and Chemical Imaging. Chem. Rev. *117*, 5146–5173. https://doi.org/10.1021/acs.chemrev.6b00448.
30. Kurouski, D., Dazzi, A., Zenobi, R., and Centrone, A. (2020). Infrared and Raman chemical imaging and spectroscopy at the nanoscale. Chem. Soc. Rev. *49*, 3315–3347. https://doi.org/10.1039/c8cs00916c.
31. Ruggeri, F.S., Flagmeier, P., Kumita, J.R., Meisl, G., Chirgadze, D.Y., Bongiovanni, M.N., Knowles, T.P.J., and Dobson, C.M. (2020). The Influence of Pathogenic Mutations in alpha-Synuclein on Biophysical and Structural Characteristics of Amyloid Fibrils. ACS Nano *14*, 5213–5222. https://doi.org/10.1021/acsnano.9b09676.
32. Ruggeri, F.S., Longo, G., Faggiano, S., Lipiec, E., Pastore, A., and Dietler, G. (2015). Infrared nanospectroscopy characterization of oligomeric and fibrillar aggregates during amyloid formation. Nat. Commun. *6*, 7831. https://doi.org/10.1038/ncomms8831.
33. Chae, J., An, S., Ramer, G., Stavila, V., Holland, G., Yoon, Y., Talin, A.A., Allendorf, M., Aksyuk, V.A., and Centrone, A. (2017). Nanophotonic Atomic Force Microscope Transducers Enable Chemical Composition and Thermal Conductivity Measurements at the Nanoscale. Nano Lett. *17*, 5587–5594. https://doi.org/10.1021/acs.nanolett.7b02404.
34. Katzenmeyer, A.M., Holland, G., Kjoller, K., and Centrone, A. (2015). Absorption spectroscopy and imaging from the visible through mid-infrared with 20 nm resolution. Anal. Chem. *87*, 3154–3159. https://doi.org/10.1021/ac504672t.
35. Ramer, G., Ruggeri, F.S., Levin, A., Knowles, T.P.J., and Centrone, A. (2018). Determination of Polypeptide Conformation with Nanoscale Resolution in Water. ACS Nano *12*, 6612–6619. https://doi.org/10.1021/acsnano.8b01425.
36. Matveyenka, M., Rizevsky, S., and Kurouski, D. (2022). Unsaturation in the Fatty Acids of Phospholipids Drastically Alters the Structure and Toxicity of Insulin Aggregates Grown in Their Presence. J. Phys. Chem. Lett. *13*, 4563–4569. https://doi.org/10.1021/acs.jpclett.2c00559.
37. Matveyenka, M., Rizevsky, S., and Kurouski, D. (2022). The degree of unsaturation of fatty acids in phosphatidylserine alters the rate of insulin aggregation and the structure and toxicity of amyloid aggregates. FEBS Lett. *596*, 1424–1433. https://doi.org/10.1002/1873-3468.14369.
38. Guo, C., Sun, L., Chen, X., and Zhang, D. (2013). Oxidative stress, mitochondrial damage and neurodegenerative diseases. Neural Regen. Res. *8*, 2003–2014. https://doi.org/10.3969/j.issn.1673-5374.2013.21.009.
39. Leuner, K., Müller, W.E., and Reichert, A.S. (2012). From mitochondrial dysfunction to amyloid beta formation: novel insights into the pathogenesis of Alzheimer's disease. Mol. Neurobiol. *46*, 186–193. https://doi.org/10.1007/s12035-012-8307-4.
40. Ogawa, O., Zhu, X., Perry, G., and Smith, M.A. (2002). Mitochondrial abnormalities and oxidative imbalance in neurodegenerative disease. Sci. Aging Knowledge Environ. *2002*, pe16. https://doi.org/10.1126/sageke.2002.41.pe16.
41. Bhattarai, K.R., Riaz, T.A., Kim, H.R., and Chae, H.J. (2021). The aftermath of the interplay between the endoplasmic reticulum stress response and redox signaling. Exp. Mol. Med. *53*, 151–167. https://doi.org/10.1038/s12276-021-00560-8.
42. Aldras, Y., Singh, S., Bode, K., Bhowmick, D.C., Jeremic, A., and O'Halloran, D.M. (2019). An inducible model of human amylin overexpression reveals diverse transcriptional changes. Neurosci. Lett. *704*, 212–219. https://doi.org/10.1016/j.neulet.2019.04.016.
43. Wilson, D.M., and Binder, L.I. (1997). Free fatty acids stimulate the polymerization of tau and amyloid beta peptides. In vitro evidence for a common effector of pathogenesis in Alzheimer's disease. Am. J. Pathol. *150*, 2181–2195.
44. Westermark, G.T., Leckström, A., Ma, Z., and Westermark, P. (1998). Increased release of IAPP in response to long-term high fat intake in mice. Horm. Metab. Res. *30*, 256–258. https://doi.org/10.1055/s-2007-978878.
45. Scollo, F., Tempra, C., Lolicato, F., Sciacca, M.F.M., Raudino, A., Milardi, D., and La Rosa, C. (2018). Phospholipids Critical Micellar Concentrations Trigger Different Mechanisms of Intrinsically Disordered Proteins Interaction with Model Membranes. J. Phys. Chem. Lett. *9*, 5125–5129. https://doi.org/10.1021/acs.jpclett.8b02241.
46. Takada, K., Kanatsuka, A., Tokuyama, Y., Yagui, K., Nishimura, M., Saito, Y., and Makino, H. (1996). Islet amyloid polypeptide/amylin contents in pancreas change with increasing age in genetically obese and diabetic

mice. Diabetes Res. Clin. Pract. *33*, 153–158. https://doi.org/10.1016/0168-8227(96)01294-6.

47. Li, D., Zhang, X., Wang, Y., Zhang, H., Song, K., Bao, K., and Zhu, P. (2022). A new polymorphism of human amylin fibrils with similar protofilaments and a conserved core. iScience *25*, 105705. https://doi.org/10.1016/j.isci.2022.105705.

48. Khemtemourian, L., Fatafta, H., Davion, B., Lecomte, S., Castano, S., and Strodel, B. (2022). Structural Dissection of the First Events Following Membrane Binding of the Islet Amyloid Polypeptide. Front. Mol. Biosci. *9*, 849979. https://doi.org/10.3389/fmolb.2022.849979.

49. Roder, C., Kupreichyk, T., Gremer, L., Schafer, L.U., Pothula, K.R., Ravelli, R.B.G., Willbold, D., Hoyer, W., and Schröder, G.F. (2020). Cryo-EM structure of islet amyloid polypeptide fibrils reveals similarities with amyloid-beta fibrils. Nat. Struct. Mol. Biol. *27*, 660–667. https://doi.org/10.1038/s41594-020-0442-4.

50. Matveyenka, M., Rizevsky, S., Pellois, J.P., and Kurouski, D. (2023). Lipids uniquely alter rates of insulin aggregation and lower toxicity of amyloid aggregates. Biochim. Biophys. Acta. Mol. Cell Biol. Lipids *1868*, 159247. https://doi.org/10.1016/j.bbalip.2022.159247.

51. Matveyenka, M., Zhaliazka, K., and Kurouski, D. (2023). Unsaturated fatty acids uniquely alter aggregation rate of α-synuclein and insulin and change the secondary structure and toxicity of amyloid aggregates formed in their presence. FASEB J. *37*, e22972. https://doi.org/10.1096/fj.202300003R.

52. Athyros, V.G., Doumas, M., Imprialos, K.P., Stavropoulos, K., Georgianou, E., Katsimardou, A., and Karagiannis, A. (2018). Diabetes and lipid metabolism. Hormones (Basel) *17*, 61–67. https://doi.org/10.1007/s42000-018-0014-8.

53. Rocha, M., Apostolova, N., Diaz-Rua, R., Muntane, J., and Victor, V.M. (2020). Mitochondria and T2D: Role of Autophagy, ER Stress, and Inflammasome. Trends Endocrinol. Metab. *31*, 725–741. https://doi.org/10.1016/j.tem.2020.03.004.

54. Ralhan, I., Chang, J., Moulton, M.J., Goodman, L.D., Lee, N.Y.J., Plummer, G., Pasolli, H.A., Matthies, D., Bellen, H.J., and Ioannou, M.S. (2023). Autolysosomal exocytosis of lipids protect neurons from ferroptosis. J. Cell Biol. *222*, e202207130. https://doi.org/10.1083/jcb.202207130.

55. Sitton, J., Pickett, D., Rodriguez, A., and Kurouski, D. (2025). Lipids determine the toxicity of human islet polypeptide aggregates in vivo. J. Biol. Chem. *301*, 108029. https://doi.org/10.1016/j.jbc.2024.108029.

56. Sitton, J., Ali, A., Osborne, L., Holman, A.P., Rodriguez, A., and Kurouski, D. (2024). Plasmalogens Alter the Aggregation Rate of Transthyretin and Lower Toxicity of Transthyretin Fibrils. J. Phys. Chem. Lett. *15*, 4761–4766. https://doi.org/10.1021/acs.jpclett.4c00868.

STAR★METHODS

KEY RESOURCES TABLE

REAGENT or RESOURCE	SOURCE	IDENTIFIER
Lipids		
Stearic acid	Ward's Science	Supplier no. SS0990-100G
Linoleic acid	TCI America Inc	cat. no. L0124
alpha-linoleic acid	Thermo Scientific	cat. no. 302825000
Arachidonic acid	Enzo Life Sciences Inc.	Supplier no. BML-FA003
Eicosapentaenoic Acid	Enzo Life Sciences Inc.	Supplier no. BML-FA001
Other chemicals		
DMSO	Sigma Aldrich	Supplier no. D8418-250 ML
HFIP	TCI America Inc	Supplier no.H0424
Thioflavin T	Sigma Aldrich	cat. no. T3516-25G
Phosphate-buffered saline (PBS)	Gibco	cat. no. 10010023
Fetal bovine serum	Thermo Fisher Scientific	cat. no. A5209501
Normocin	InvivoGen	cat. no. ant-nr-1
0.25% Trypsin in 2.21 mM EDTA and 1x Sodium Bicarbonate Buffer	Corning	cat. no. MT25053CI
JC-1 Assay Kit	Thermo Fisher Scientific	cat. no. M34152A
ROS detection reagent	Thermo Fisher Scientific	cat. no. C10422
GeneJET RNA Purification Kit	Thermo Scientific	cat. no. K0732
Random Primers	Invitrogen	cat. no. 48190011
SuperScript II Reverse Transcriptase	Invitrogen	cat. no. 18064014
Luna Universal qPCR Master Mix	New England Biolabs	cat. no. M3003
SuperSignal™ West Femto Maximum Sensitivity Substrate	Thermo Scientific	cat. no. 34094
5-fluorodeoxyuridine (FUDR)	Thermo Scientific	cat. no. 2276050000
Difco Agar	BD	cat. no. DF0812-17-9
Luria Broth Base	Invitrogen	cat. no. 12795084
Peptone	Fisher Scientific	cat. no. BP1420-500
Sodium Chloride	Sigma Aldrich	cat. no. S9888-1 KG
Potassium Phosphate, Dibasic	Fisher Scientific	cat. no. P290-500
Potassium Phosphate, monobasic	Fisher Scientific	P285-500
Cholesterol (ovine)	Avanti Polar Lipids	cat. no. 700000P-5g
Magnesium Sulfate	J.T. Baker	cat. no. 2506-01
Calcium Chloride Dihydrate	Sigma Aldrich	cat. no. 21102-1 KG-F
Proteins and antibodies		
Human IAPP 1-37	Eurogentec	cat. no. AS-60254-1
Rodent IAPP	Eurogentec	cat. no. AS-60253-1
A11 Antibody	Invitrogen	cat. no. AHB0052; RRID: AB_10376183
Goat anti-Rabbit IgG HRP	Invitrogen	cat. no. 31460; RRID: AB_2534770
Cells		
N27 cells	Millipore	cat. no. SCC048, RRID:CVCL_D584
BRIN-BD11 pancreatic β cells	Millipore	cat. no. 10033003-1VL, RRID:CVCL_6811
OP50 *E. coli*	Internal stock	–
Plastic		
96-well plates	Sarstedt	cat. no.83.3924.300

(*Continued on next page*)

Continued

REAGENT or RESOURCE	SOURCE	IDENTIFIER
Software and algorithms		
JASP	University of Amsterdam	version 0.19.0.0
AIST-NT	AIST-NT	version 3.5.158
IApro	AIST-NT	version 3.4.2
Fiji/ImageJ	ImageJ	version 1.54f
Perkin Elmer Spectrum software	Perkin Elmer	version 10.4.4
Bruker Analysis Studio	Bruker	version 3.17
MATLAB 2022a	MathWorks	version 9.12
Eigenvector PLS Toolbox	Eigenvector	version 9.0
GRAMS/AI	Thermo Scientific	version 9.3
BD FACSDiva Software	BD Biosciences	version 8.0.1
QuantStudio Real-Time PCR Software	Thermo Fisher Scientific	version 1.7.2

EXPERIMENTAL MODELS AND STUDY PARTICIPANT DETAILS

Cell culture

BRIN-BD11 pancreatic β-cells and N27 dopaminergic neurons were obtained from Millipore and cultured in RPMI 1640, 10% FBS at 37°C in a 5% CO_2 incubator. Cell lines did not undergo further authentication outside of that provided by the supplier. Tests for mycoplasma were performed via PCR if contamination was suspected.

Caenorhabditis elegans

DMH46 strain of *C. elegans* was a kind gift from Dr. Damien O'Halloran of George Washington University. N2 wildtype worms were a kind gift from Dr. Michael Polymenis of Texas A&M University. N2 wildtype and DMH46 nematodes were maintained on NGM plates seeded with OP50 *E. coli* at 17 °C before and at 25 °C during experiments. Hermaphroditic worms were utilized in all experiments to eliminate sex-determined influences in organism lifespan.

Escherichia coli OP50 *E. coli* was a kind gift from Dr. Michael Polymenis of Texas A&M University. OP50 cultures were grown in LB broth (Invitrogen) until late Log growth phase. Bacteria was then collected and centrifuged and resuspended in 10% of the original culture volume to yield a 10x concentrated stock before seeding onto NGM plates and UV irradiating.

METHOD DETAILS

Fatty acid micelle preparation

Stearic acid was purchased from Ward's Science in solid form. Linoleic acid was purchased from TCI America Inc. and alpha-linoleic acid was purchased from Thermo Scientific, both as oils. Arachidonic acid and eicosapentoic acid were purchased from Enzo Life Sciences Inc. as oils. All FAs were dissolved in DMSO before being diluted into 1x PBS pH 7.4 to a final concentration of 4 mM FA, 1% DMSO, in 1x PBS pH 7.4. All FA solutions underwent multiple freeze-thaw and sonication cycles, careful to avoid unnecessary heat and light exposure to prevent oxidation and degradation of the FAs. All FA micelle solutions were made fresh before each experiment to ensure FA integrity. 1x PBS with 1% DMSO was prepared and used for IAPP aggregation in the FA-free environment and as a vehicle control in toxicity assays.

Protein sourcing and preparation

Protein preparation was completed as previously described.[55] Human IAPP 1–37 (Eurogentec) or Rodent IAPP (Eurogentec) was dissolved in HFIP at a concentration of 1 mg/mL and incubated at 4°C for 24 h to dissolve any preformed aggregates. This solution was then filtered through a 0.22 μm filter and aliquoted into .2 mg aliquots. The HFIP was removed by drying under nitrogen gas to yield a thin protein film. The dried protein was then freeze-dried for 48 h then stored at −20°C for no more than 1 month.

Thioflavin T (ThT) kinetics

Kinetic experiments were prepared as previously described.[55] 100 μM IAPP stock solution was prepared and kept on ice. FA conditions were prepared by mixing the appropriate volume of FA stock with 1x PBS pH 7.4 in a 1.5 mL tube. ThT was then added for a final concentration of 50 μM per well. Each condition was aliquoted into a pre-chilled 96 well plate, and the IAPP stock solution was added last. The final volume of each well was 105 μL with 50 μM ThT, 400 μM FA, and 20, 30, or 40 μM IAPP and final pH of 7.4. The FA-free condition was incubated with 1x PBS with 1% DMSO in place of the FA stock. 96 well plates were incubated in a Tecan

Spark plate reader (Tecan) at 37°C for 24 h with readings taken at 450 nm excitation and 495 nm emission every 10 min. All conditions were performed in triplicates. Kinetic curves shown are the average of these triplicates.

Atomic force microscopy (AFM)

Samples were prepared as described in the ThT Kinetics experiments, with ThT being replaced with 1x PBS, and incubated for 48 h at 37°C with gentle agitation. Samples were deposited onto P-type silicon wafers and dried ambiently. The samples were then rinsed with DI water and dried under nitrogen gas. Images were recorded using AIST-NT-HORIBA system in tapping mode and processed using the AIST-NT program. Height data were acquired after processing by profile measurement focusing on acquiring height for as many separate fibrils as possible. Fibrils that had varying thickness were measured in multiple locations to accurately represent the whole population, and thicker aggregates that appeared to be multiple fibrils stacked together were avoided in measurements. At least 30 heights were taken per sample and multiple images were scanned for each sample.

A11 dot-blot analysis

Samples were prepared identically to those used for AFM. A 1:2 serial dilution was performed in 1x TBS before samples were applied to a prewet 0.4 μm nitrocellulose membrane (Bio-Rad) using a Bio-Rad Bio-Dot Apparatus (Bio-Rad) using the manufacturer's instructions. The membrane was subsequently blocked with 1% BSA in 1x TBS and washed three times with TBS with 0.05% Tween 20 (TBST). The A11 antibody (Invitrogen) was diluted to a concentration of 1 μg/mL and 100 μL was added to each well. After antigen binding, the membrane was washed again three times with TBST before applying 100 μL Goat anti-Rabbit IgG (H + L) Secondary Antibody, HRP (Invitrogen) diluted in 1x TBS to a final concentration of 0.18 μg/mL. The membrane was then washed again three times with TBST and rinsed with 1x TBS two times before developing. The membrane was developed with SuperSignal West Femto Maximum Sensitivity Substrate (Thermo Scientific) using the manufacturer's instructions before exposing. The membrane was exposed and imaged using GE Amersham Imager 600 Luminescence Image Analyzer (General Electric). Integrated density of each dot was measured in Fiji/ImageJ after subtracting background and normalized to the integrated density of IAPP alone at the highest tested concentration.

Attenuated total reflectance Fourier transform infrared (ATR-FTIR) spectroscopy

Samples prepared for FTIR spectroscopy as described for AFM. Samples were deposited onto the crystal of 100 FTIR spectrometer (PerkinElmer) equipped with the ATR module and dried at room temperature. 3 spectra consisting of 4 coaveraged spectral scans were collected from each sample. The 3 spectra were then averaged for each sample and normalized to 1.

Nano-IR spectroscopy

Nano-IR spectra were collected as previously described.[56] Samples were prepared as described for AFM and deposited on gold-coated silicon wafers. 30 spectra comprised of 3 coaveraged spectra each were collected from each sample, targeting as many individual fibrils as possible. Spectra were processed using the PLS toolbox in MATLAB, and Gaussian peak fitting was conducted in GRAMS/AI Spectroscopy Software within the Amide I region of the spectra. Parallel β-sheet was considered from 1610 to 1635 cm^{-1}, α-helix, β-turn, and random coil from 1640 to 1670 cm^{-1}, and anti-parallel β-sheet from 1675 to 1700 cm^{-1}. Peak area for each band corresponding to their respective secondary-structure was normalized to the total peak area from all three spectral bands of focus to obtain the relative intensity and quantify relative secondary-structure.

Cell toxicity assays

ROS and JC-1 assays were performed as previously described.[55] Samples for cell toxicity were prepared as described for AFM. BRIN-BD11 pancreatic β-cells and N27 dopaminergic neurons in RPMI 1640, 10% FBS, and Anti-Anti were seeded in a 96 well plate (30,000 cells/well) and allowed to reach ~80% confluence (24 h). Once confluent, cell media was changed to DMEM, 2.5% FBS, Anti-Anti and IAPP:FA samples were added to a final concentration of 12 μM, 9 μM, or 6 μM IAPP and 120 μM FAs. Vehicle control cells were treated with an equal volume of 1x PBS with 1% DMSO. Samples to test the effects of FAs alone were treated the same was as those with IAPP, replacing the volume of IAPP stock solution in each sample with an equal volume of 1x PBS. Cells were incubated at 37°C with 5% CO_2 for 24 h before dying for ROS and JC-1. Cells were dyed following the manufacturers provided instructions. All conditions were completed in triplicates with three independent cultures per cell line.

Real time quantitative PCR (qPCR)

qPCR was performed as previously described.[55] Cells were cultured and treated as described for cell toxicity assays. RNA was extracted from the treated cells and cDNA synthesis was performed using SuperScript II Reverse Transcriptase (Invitrogen) with random primers (Invitrogen). Specific primers were designed with sequences optimized for the specific target genes and to be compatible with qPCR amplification conditions. qPCR reactions were performed using a Quantstudio 7 Flex (Applied Biosystems). PCRs were performed in 35–40 cycles, and GADPH was used as a housekeeping gene. Relative gene expression was calculated using the comparative Ct method (2^−ΔΔCt). The relative gene expression levels were calculated and presented as fold changes compared with the control samples. Each experiment was performed in triplicates.

Caenorhabditis elegans

C. elegans experiments were performed as previously described.[55] N2 wildtype and DMH46 nematodes were maintained on NGM plates seeded with OP50 *E. coli* at 17°C until unhatched eggs were visible. The worms were then age synchronized and allowed to reach day 1 adulthood before being moved to experimental plates containing 5-fluorodeoxyuridine (FUDR). Experimental plates were supplemented with FAs by mixing FAs of interest with 10X OP50 *E. coli* which was then seeded on to the plates, dried, and UV irradiated. A final concentration of 0.2 mg FA per plate was added, and the FA free environment was seeded with OP50 only. Temperature was then increased to 25°C to induce IAPP expression in DMH46 nematodes at the same time as exposure to FAs. N2 nematodes were incubated at 25°C once moved to FA conditioned plates to prevent influence of temperature on lifespan. Each condition utilized 5 plates with 10 hermaphroditic worms on each plate, totaling a population of 50 worms per condition. Kaplan-Meier survival analysis and statistical analysis were performed in JASP statistical software.

QUANTIFICATION AND STATISTICAL ANALYSIS

Raw data was exported as CSV files. Raw data files were uploaded to Microsoft Office 365 Excel for initial viewing before being uploaded to the respective software. All statistics were performed using JASP version 0.19.0.0, and the specific test utilized can be found in the respective figure legend and methods with the corresponding sample size, dispersion, and precision. ThT Kinetic data was plotted in Microsoft Office 365 Excel, and overlaid line plot in JASP 0.19.0.0. AFM images were acquired and processed using AIST-NT version 3.5.158 and IApro version 3.4.2, respectively. Height data was acquired using IApro version 3.4.2, plotted, and tested statistically using JASP version 0.19.0.0. A11 dot blot data was analyzed using Fiji/ImageJ version 1.54f (Java 1.8.0_322(64-bit)) then platted using JASP 0.19.0.0. ATR-FTIR spectra were collected using PerkinElmer Spectrum software version 10.4.4, then plotted in Microsoft Office 365 Excel. AFM-IR spectra were acquired using Bruker Analysis Studio version 3.17, then subsequently processed in MATLAB 2022a version 9.12 using Eigenvector PLS Toolbox version 9.0 and plotted in Microsoft Office 365 Excel. The resulting AFM-IR spectra from MATLAB were peak fitted in GRAMS/AI version 9.3, plotted in Microsoft Office 365 Excel, and analyzed statistically using JASP version 0.19.0.0. ROS and JC-1 data was acquired using BD FACSDiva Software Version 8.0.1, plotted using Microsoft Office 365 Excel and JASP version 0.19.0.0, and analyzed statistically using JASP version 0.19.0.0. qPCR data was acquired using QuantStudio Real-Time PCR Software version 1.7.2 and subsequently processed and plotted in Microsoft Office 365 Excel. Kaplan-Meir survival curves were calculated and plotted using JASP version 0.19.0.0, with the same software used for statistical testing and confidence interval calculations.